PAPER • OPEN ACCESS

Scattering fingerprints of two-state dynamics

To cite this article: Cai Dieball *et al* 2022 *New J. Phys.* **24** 023004

New Journal of Physics
The open access journal at the forefront of physics

Deutsche Physikalische Gesellschaft DPG
IOP Institute of Physics

Published in partnership with: Deutsche Physikalische Gesellschaft and the Institute of Physics

OPEN ACCESS

RECEIVED
27 October 2021

REVISED
20 December 2021

ACCEPTED FOR PUBLICATION
6 January 2022

PUBLISHED
9 February 2022

PAPER

Scattering fingerprints of two-state dynamics

Cai Dieball[1], Diego Krapf[2], Matthias Weiss[3] and Aljaž Godec[1,*]

[1] Mathematical BioPhysics Group, Max Planck Institute for Biophysical Chemistry, Göttingen, Germany
[2] Electrical and Computer Engineering and School of Biomedical Engineering, Colorado State University, Fort Collins, CO, United States of America
[3] Experimental Physics I, University of Bayreuth, Bayreuth, Germany
[*] Author to whom any correspondence should be addressed.

E-mail: agodec@mpibpc.mpg.de

Keywords: dynamic structure factor, intermediate scattering function, diffusion, fractional Brownian motion, Gaussian network model, segmentation, two-channel processes

Abstract

Particle transport in complex environments such as the interior of living cells is often (transiently) non-Fickian or anomalous, that is, it deviates from the laws of Brownian motion. Such anomalies may be the result of small-scale spatio-temporal heterogeneities in, or viscoelastic properties of, the medium, molecular crowding, etc. Often the observed dynamics displays multi-state characteristics, i.e. distinct modes of transport dynamically interconverting between each other in a stochastic manner. Reliably distinguishing between single- and multi-state dynamics is challenging and requires a combination of distinct approaches. To complement the existing methods relying on the analysis of the particle's mean squared displacement, position- or displacement-autocorrelation function, and propagators, we here focus on 'scattering fingerprints' of multi-state dynamics. We develop a theoretical framework for two-state scattering signatures—the intermediate scattering function and dynamic structure factor—and apply it to the analysis of simple model systems as well as particle-tracking experiments in living cells. We consider inert tracer-particle motion as well as systems with an internal structure and dynamics. Our results may generally be relevant for the interpretation of state-of-the-art differential dynamic microscopy experiments on complex particulate systems, as well as inelastic or quasielastic neutron (incl. spin-echo) and x-ray scattering probing structural and dynamical properties of macromolecules, when the underlying dynamics displays two-state transport.

1. Introduction

Transport in complex systems such as disordered media [1], biological cells [2, 3], and cell membranes [4, 5], frequently deviates from the laws of Brownian motion that govern the dynamics of particles in simple media and at high dilution. The reason for the deviation from the paradigmatic Brownian behavior may be sought in spatial obstruction and/or macromolecular crowding [2, 3, 5], viscoelastic properties of the medium [6–10], and spatial heterogeneities [11, 12], to name but a few. Over the years a multitude of approaches have emerged to characterize anomalous diffusion from different perspectives, and in particular to distinguish between different modes of anomalous diffusion (for excellent reviews see e.g. [3, 4, 13–15]).

An important class of anomalous diffusion processes are multi-state dynamics—dynamics that depend on the instantaneous value of an internal state. Examples of multi-state dynamics include stochastically gated diffusion-controlled reactions [16–20], intermittent molecular search processes underlying cellular gene regulation [21–23], or the center of mass diffusion of (un)folding proteins [24] or growing polymers [25], the anomalous diffusion of membrane proteins [26], as well as tracer diffusion in heterogeneous environments [27, 28], and most recently also in mammalian cells [29, 30].

Notwithstanding all progress in the development of analytical tools [2, 3, 13, 15, 31] it often remains challenging to conclusively distinguish between different modes of motion observed in experiments [32], and in particular to conclusively identify multi-state transport [33–35]. To this end, we focus on scattering

fingerprints of multi-state dynamics, that is, on the intermediate scattering function (ISF) and dynamic structure factor (DSF), observables that are typically monitored in neutron and x-ray scattering experiments (for applications in the context of biophysical systems see e.g. [36–39]). The ISF and the DSF were originally identified as key observables in scattering experiments by van Hove [40]. While the ISF was initially introduced as an auxiliary observable in the study of the DSF, more recent methods, such as neutron spin echo (NSE) spectroscopy [41–44], as well as modern (colloidal) particle-tracking techniques, such as differential dynamic microscopy (DDM) [45–47] or Fourier imaging correlation spectroscopy (FICS) [48–50], probe the ISF directly.

Motivated by recent experimental observations (see e.g. [29, 30, 51]) our aim is to employ the ISF and DSF in the analysis of multi-state transport, more precisely, of two-state dynamics. By combining theory and particle-tracking experiments in living cells we consider inert tracer-particle dynamics as well as systems with internal degrees of freedom. Our results may be relevant for the interpretation of DDM experiments on complex particulate systems, as well as neutron and x-ray scattering, when the underlying dynamics displays two-state transport.

2. Theory

2.1. Intermediate scattering function and the dynamic structure factor

The fundamental quantities, the ISF and DSF, are calculated from the so-called van Hove function $G(\vec{r},t)$, which is a generalized pair distribution function [40, 52]. In the absence of quantum effects $G(\vec{r},t)$ is the density–density time-correlation function that may be interpreted as the average number of particles (scatterers) β in a region $\mathrm{d}\vec{r}$ around a point $\vec{r}+\vec{r}'$ at time t given that there was a particle (scatterer) α at a point $\vec{r}'$ at time $t=0$ (whereby the initial condition $\vec{r}'$ is averaged out),

$$G^{\alpha\beta}(\vec{r},t)=\langle\delta(\vec{r}_\beta(t)-\vec{r}_\alpha(0)-\vec{r})\rangle. \tag{1}$$

The brackets denote the average over an appropriate ensemble that we will specify below. For the sake of simplicity we here focus exclusively on systems of non-interacting molecules, which, however, may possess internal degrees of freedom. Depending on whether $\alpha=\beta$ or not (i.e. whether we consider scattering events at an individual or two distinct scatterers) the van Hove function splits into an incoherent part (self-part, $\alpha=\beta$) that probes single-scatterer motions, and a coherent part (sum of distinct-part, $\alpha\neq\beta$, and self-part) probing collective motions [52]. More precisely,

$$G_{\mathrm{inc}}(\vec{r},t)=\frac{1}{N}\sum_{\alpha=1}^{N}G^{\alpha\alpha}(\vec{r},t), \tag{2}$$

$$G_{\mathrm{coh}}(\vec{r},t)=\frac{1}{N}\sum_{\alpha,\beta=1}^{N}G^{\alpha\beta}(\vec{r},t), \tag{3}$$

where the sum runs over all N scattering centers within a molecule and we will in addition average over an ensemble of statistically independent trajectories of the molecule (in fact over an ensemble of many such molecules) that we denote by $\langle\cdot\rangle$. Depending on the experimental setup $G_{\mathrm{inc}}(\vec{r},t)$ and $G_{\mathrm{coh}}(\vec{r},t)$ may [53] or may not be monitored separately.

The intermediate scattering function (ISF; mathematically the characteristic function of displacements[4]) measured in NSE, DDM and FICS is the spatial Fourier transform of $G^{\alpha\beta}(\vec{r},t)$,

$$F^{\alpha\beta}(\vec{q},t)=\int\mathrm{d}^3r\,G^{\alpha\beta}(\vec{r},t)\mathrm{e}^{-\mathrm{i}\vec{q}\cdot\vec{r}}=\langle\mathrm{e}^{-\mathrm{i}\vec{q}\cdot(\vec{r}_\beta(t)-\vec{r}_\alpha(0))}\rangle, \tag{4}$$

while the DSF that is measured in inelastic/quasielastic scattering experiments is the space-and-time Fourier transform of $G^{\alpha\beta}(\vec{r},t)$, i.e.

$$S^{\alpha\beta}(\vec{q},\omega)=\frac{1}{2\pi}\int_{-\infty}^{\infty}\mathrm{d}t\,\mathrm{e}^{\mathrm{i}\omega t}F^{\alpha\beta}(\vec{q},|t|)=\frac{1}{\pi}\int_{0}^{\infty}\mathrm{d}t\,\cos(\omega t)F^{\alpha\beta}(\vec{q},t), \tag{5}$$

or alternatively defined via the Laplace transform $\widehat{f}(s)\equiv\int_0^\infty\mathrm{e}^{-st}f(t)\mathrm{d}t$ as $S^{\alpha\beta}(\vec{q},\omega)=\pi^{-1}\Re[\widehat{F^{\alpha\beta}}(\vec{q},s=-\mathrm{i}\omega)]$, where $\Re$ denotes the real part.

[4] If moments of the displacement are finite, the ISF as a function of q contains the complete information about the statistics of the displacements.

In scattering experiments the arguments $\vec{q}$ and ω correspond to the momentum and energy transfer and the DSF is proportional to the measured intensity [40]. In the next step we develop results for $F^{\alpha\beta}(\vec{q},t)$ and $S^{\alpha\beta}(\vec{q},\omega)$ for systems displaying two-state dynamics.

2.2. Two-state dynamics

Assuming two distinct dynamic 'states' interconverting in continuous time in a Markovian manner with rates $k_1, k_2 > 0$, that is, according to the master equation $\dot{\vec{p}}(t) = K\vec{p}(t)$ with transition rate matrix

$$K = \begin{bmatrix} -k_1 & k_2 \\ k_1 & -k_2 \end{bmatrix}. \tag{6}$$

Using

$$p_1^{\mathrm{eq}} \equiv \frac{k_2}{k_1+k_2}, \qquad p_2^{\mathrm{eq}} \equiv \frac{k_1}{k_1+k_2}, \tag{7}$$

the jump-propagator is diagonalized as

$$\exp(Kt) = \begin{pmatrix} p_1^{\mathrm{eq}} \\ p_2^{\mathrm{eq}} \end{pmatrix}(1,1) + \mathrm{e}^{-(k_1+k_2)t}\begin{pmatrix} 1 \\ -1 \end{pmatrix}\left(p_2^{\mathrm{eq}}, -p_1^{\mathrm{eq}}\right). \tag{8}$$

We now assume $N = 1$ and drop the indices α, β; the case $N > 1$ is discussed in appendix A. Let $G_j(\vec{r},t)\psi_j(t)$ denote the joint density to observe a displacement $\vec{r}$ in a time t in dynamical state j without changing the state, where $G_j(\vec{r},t)$ denotes the van Hove function for the dynamics in a single state j. Its Fourier–Laplace transform will be denoted by

$$\widehat{(F\psi)}_j \equiv \widehat{(F\psi)}_j(\vec{q},s) \equiv \int \mathrm{d}^3 r \int_0^\infty \mathrm{d}t\, \mathrm{e}^{-st-\mathrm{i}\vec{q}\cdot\vec{r}} G_j(\vec{r},t)\psi_j(t). \tag{9}$$

Often the change of state erases all memory in the sense that the propagation within each sojourn can be assumed to be independent of the configuration just before the switch [54], as in the case e.g. when the dynamics in both states is translation invariant. In this case the DSF and ISF of the complete two-state dynamics can be obtained following reference [54] by a direct summation over all possible realizations of sojourns until time t (for the derivation see appendix A). The Fourier–Laplace transform of the complete two-state propagator, $G(\vec{r},t)$, in this case reads

$$\widehat{F}(\vec{q},s) = \frac{p_1\widehat{(F\psi)}_1\left[1+k_1\widehat{(F\psi)}_2\right] + p_2\widehat{(F\psi)}_2\left[1+k_2\widehat{(F\psi)}_1\right]}{1-k_1k_2\widehat{(F\psi)}_1\widehat{(F\psi)}_2}, \tag{10}$$

where $p_{1,2}$ denote the initial occupation of states. The DSF henceforth follows immediately using

$$S(\vec{q},\omega) = \frac{1}{\pi}\,\Re[\widehat{F}(\vec{q},-\mathrm{i}\omega)]. \tag{11}$$

The problem of determining the ISF and DSF for two-state dynamics with 'complete memory erasure' upon each change of state thus boils down to determining $\widehat{(F\psi)}_{1,2}(\vec{q},s)$ in equation (9) for the specific example under consideration. In case there is no complete memory erasure (see protein (un)folding example section 3.4) one must solve the specific model at hand using a dedicated method or resort to approximations. In the following we address a set of insightful and experimentally relevant scenarios of two-state diffusion.

3. Results

3.1. Two-state diffusion

In the first example we assume that the molecule/tracer particle undergoes free Brownian motion with a diffusion coefficient that randomly switches between values D_1 and D_2 in a Markovian fashion with rates k_1 and k_2, implying the distribution $\psi_j(t) = \mathrm{e}^{-k_j t}$ of sojourn times in the respective states. This situation arises in the context of tracer diffusion in heterogeneous media (see e.g. [20, 27, 28]). Note that assuming sojourn times to be independent of the dynamics within the individual states is not always justified. In particular, we here assume an 'annealed heterogeneity' (see e.g. [12]). This may occur when the medium is translationally invariant such as in the case of a state change triggered by the reversible binding to a homogeneously distributed mobile species. In general this does not apply to quenched heterogeneous media, except in cases where a system is observed under equilibrated conditions [55].

The Fourier–Laplace transform of $G_j(\vec{r},t)\psi_j(t)$ defined in equation (9) reads

$$\widehat{(F\psi)}_j(\vec{q},s) = \widehat{(F\psi)}_j(q,s) = \frac{1}{s+q^2D_j+k_j}, \tag{12}$$

where $q^2 \equiv \vec{q}\cdot\vec{q}$. Plugging equation (12) into equation (10) the Fourier–Laplace image of the complete propagator for two-state diffusion can be written as

$$\widehat{F}(q,s) = \frac{s+q^2(p_1D_2+p_2D_1)+k_1+k_2}{(s+q^2D_1+k_1)(s+q^2D_2+k_2)-k_1k_2}, \tag{13}$$

with a general initial condition $p_{1,2}$. Defining

$$\mu_\pm(q) = \frac{q^2(D_1+D_2)+k_1+k_2}{2} \pm \sqrt{\frac{[q^2(D_1-D_2)+k_1-k_2]^2}{4}+k_1k_2}, \tag{14}$$

introducing the auxiliary function

$$\varphi(q) \equiv \frac{q^2(p_1D_2+p_2D_1)+k_1+k_2-\mu_-(q)}{\mu_+(q)-\mu_-(q)}, \tag{15}$$

and inverting into the time domain we finally obtain

$$F(q,t) = [1-\varphi(q)]\mathrm{e}^{-\mu_+(q)t} + \varphi(q)\mathrm{e}^{-\mu_-(q)t}, \tag{16}$$

$$S(q,\omega) = \frac{1}{\pi}\,\Re[\widehat{F}(q,-\mathrm{i}\omega)] = \frac{1}{\pi}\frac{[1-\varphi(q)]\mu_+(q)}{\omega^2+\mu_+^2(q)} + \frac{1}{\pi}\frac{\varphi(q)\mu_-(q)}{\omega^2+\mu_-^2(q)}. \tag{17}$$

In contrast, in the case when the two states co-evolve as a 'frozen mixture'—an ensemble consisting of two types of molecules that do not interconvert between each other—with the state occupations $p_{1,2}$ we have $F_{\mathrm{mix}}(q,t) = p_1\,\mathrm{e}^{-q^2D_1t} + p_2\,\mathrm{e}^{-q^2D_2t}$. This frozen mixture will throughout be denoted by the subscript 'mix', and is the limit of equation (16) in the case of slow switching rates $k_1+k_2 \ll q^2D_{1,2}$, see appendix B.

It is also instructive to inspect the fast-switching limit, $k_1+k_2 \gg q^2D_{1,2}$, where we find (for details see appendix B) $\mu_+(q) \simeq q^2D_{\mathrm{eff}} \equiv p_1^{\mathrm{eq}}D_1 + p_2^{\mathrm{eq}}D_2$ and $\mu_-(q) \simeq k_1+k_2 \gg q^2D_{1,2}$, which implies simple diffusion with an effective diffusion coefficient in agreement with intuition.

Our aim here is to demonstrate that the analysis allows to distinguish between single-state dynamics, two-state switching diffusion and the 'frozen mixture' with the same stationary probabilities as long as the switching rates are not too fast or too slow, which would give rise to the aforementioned (fast-switching) effective diffusion and 'frozen mixture', respectively.

For such moderate switching rates the ISF shown in figure 1(a) and the DSF in figure 1(b) indeed reveal distinctive characteristics of two-state diffusion (dashed lines) when compared to the 'frozen mixture' (black full line) as well as the two individual diffusive states (blue and green full lines, respectively). To reduce these differences to a single observable we inspect the half width at half the maximum (HWHM) of the quasielastic peak as a function of the switching rate (that for simplicity we set to be symmetric, $k_1 = k_2 \equiv k$) for different initial conditions. The HWHM is determined from equation (17) by setting $S(q,\omega_{\mathrm{HWHM}}) = S(q,0)/2$ and solving the corresponding bi-quadratic equation for ω_{HWHM}. The results for ω_{HWHM} are shown in figure 1(c) and together with figures 1(a) and (b) confirm that the DSF and ISF can reliably distinguish between a 'non-communicating', frozen superposition of dynamic modes and two-state diffusion as long as the switching rates are not too fast or too slow.

Note that for an isotropic Gaussian process we have $F(q,t) = \mathrm{e}^{-q^2\langle[\vec{r}(t)-\vec{r}(0)]^2\rangle/2d}$ and hence ISF contains exactly the same information as the mean squared displacement (MSD) $\langle[\vec{r}(t)-\vec{r}(0)]^2\rangle$. For the individual states as well as for effective diffusion the dynamics is Gaussian. However, two-state dynamics is typically non-Gaussian [29] and the ISF provides more information about the dynamics. Note, moreover, that the MSD of the two-state process reflects (normal) diffusion with effective diffusivity D_{eff} for all switching rates and thus alone cannot reveal underlying two-state dynamics. In the next example we turn to the switching between two subdiffusive states.

3.2. Two-state fractional Brownian motion

Tracer transport in complex, dynamic and/or heterogeneous media such as living cells is often found to be anomalous [2, 3, 13, 56]. Particularly interesting are situations with stochastically interconverting anomalous diffusion processes such as the two-state anti-persistent (i.e. subdiffusive) fractional Brownian motion (FBM) observed in recent experiments on mammalian cells [29, 30]. To be more precise, a systematic analysis of the motion of quantum dots immersed in the cytoplasm of living mammalian cells

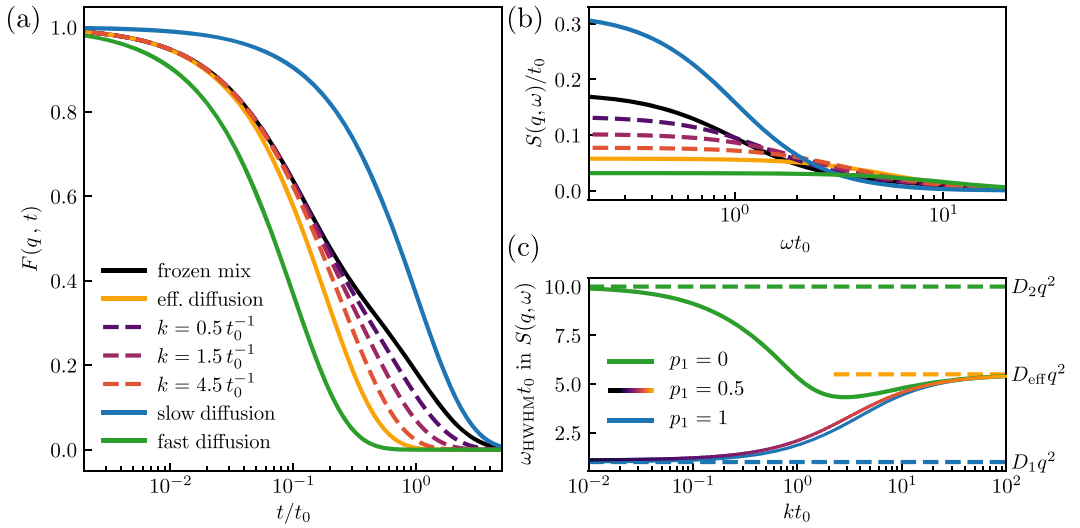

Figure 1. (a) ISF $F(q,t)$ for free diffusion switching between diffusion constants D_1 and $D_2 = 10D_1$ with switching rates $k_1 = k_2 = k$ evolving from an initial equilibrium occupation $p_1^{\mathrm{eq}} = p_2^{\mathrm{eq}} = 0.5$ and time t measured in units of $t_0 = 1/D_1q^2$. The ISF for different switching rates are shown along with the limits of the frozen mix ($k \to 0$, black curve) and the effective diffusion ($k \to \infty$, yellow curve). (b) Dynamical structure factor corresponding to the ISF in (a). (c) Half width at half maximum (HWHM) of the DSF from (b) are shown along with the HWHMs of the blue, green and yellow curves in (b) (dashed lines). To compare with a non-equilibrium initial occupation, the HWHM for initial occupation $p_1 = 0$ and $p_1 = 1$ are also shown (green and blue lines, respectively).

revealed two-state subdiffusive FBM with exponent $\alpha < 1$ but with a stochastically switching anomalous diffusion coefficient $C_{1,2}$ [29]. Here we determine the DSF and ISF for the process as complementary observables and apply them to the analysis of data obtained in [29] focusing on latrunculin-treated cells. Untreated cells had been seen to feature the same dynamics [29]. Note that here a Markov switching between the two states coexists with non-Markovian subdiffusion in each of the two states, respectively, with a MSD $\langle[\vec{r}(t) - \vec{r}(0)]^2\rangle_j = 2dC_jt^{\alpha_j}$ where d (here equal two) is the dimensionality of the system, and $\langle\cdot\rangle_j$ denotes the average over an ensemble of FBMs with exponent α_j and coefficient C_j. Thus, there is an inherent ambiguity in how to treat memory upon each jump. Here, in contrast to the original publication [29], we assume for convenience that the memory in $\vec{r}(t)$ is erased upon each change of state, which allows us to use the result in equation (10). Notably, this choice does not affect the inferred two-state FBM, which further substantiates the robustness of the proposed model.

We first treat the problem theoretically. The d-dimensional FBM is an isotropic and translationally invariant Gaussian process. Thus the ISF of FBM is the characteristic function of a Gaussian process $F_j(q,t) = \exp(-q^2\langle[\vec{r}(t) - \vec{r}(0)]^2\rangle_j/2d)$. Within a sojourn in state $j = 1, 2$ the characteristic function of the displacement $\vec{r}$ in a time t without changing the state is $F_j(q,t)\psi_j(t) = \exp(-[q^2C_jt^{\alpha_j} + k_j]t)$. Its Laplace transform $\widehat{(F\psi)}_j(q,s)$ may be written in terms of Meijer G-functions in appendix C (see equation (C.3)). Plugging the result for $\widehat{(F\psi)}_j(q,s)$ into equation (10) yields the Laplace-transformed ISF, which we invert numerically into the time domain. The DSF is in turn obtained fully analytically by setting $s = -\mathrm{i}\omega$ and taking the real part as in equation (11).

The model contains six parameters $C_1, C_2, k_1, k_2, \alpha_1, \alpha_2$ to be determined. To minimize overfitting we fix three parameters by considering the short-time behavior of the MSD, see dashed line in figure 2(a). We see that the short time MSD (i.e. prior to any change of state) is well described by simple subdiffusion with $\alpha = 0.5$, and we thus fit at the first 10 seconds yielding $C_{\mathrm{short}} = 0.0083\ \mu\mathrm{m}^2\ \mathrm{s}^{-1/2}$. To reduce the number of free parameters, we constrain ourselves to exactly reproduce this short-time behavior at times sufficiently short to not be influenced by transitions, i.e. we fix $\alpha_1 = \alpha_2 = 0.5$ and $p_1^{\mathrm{eq}}C_1 + p_2^{\mathrm{eq}}C_2 = C_{\mathrm{short}}$ (recall $p_1^{\mathrm{eq}} = k_2/(k_1 + k_2)$ from equation (7)). This leaves three free parameters which we determine by a least-squares fit simultaneously at $q = 3\ \mu\mathrm{m}^{-1}$ and $q = 7\ \mu\mathrm{m}^{-1}$. The fitting yields $C_1 = 0.002\ \mu\mathrm{m}^2\ \mathrm{s}^{-1/2}$, $C_2 = 0.052\ \mu\mathrm{m}^2\ \mathrm{s}^{-1/2}$, $k_1 = 0.009\ \mathrm{s}^{-1}$, $k_2 = 0.063\ \mathrm{s}^{-1}$.

For the case $\alpha_j = 1/2$ the Fourier–Laplace transform of the joint density to observe a displacement $\vec{r}$ in a time t without changing the state reads (see appendix C)

$$\widehat{(F\psi)}_j(q,s) = \frac{1}{s + k_j} - \frac{\sqrt{\pi}q^2C_j}{2(s + k_j)^{3/2}}\,\mathrm{erfcx}\left(\frac{q^2C_j}{2\sqrt{s + k_j}}\right), \tag{18}$$

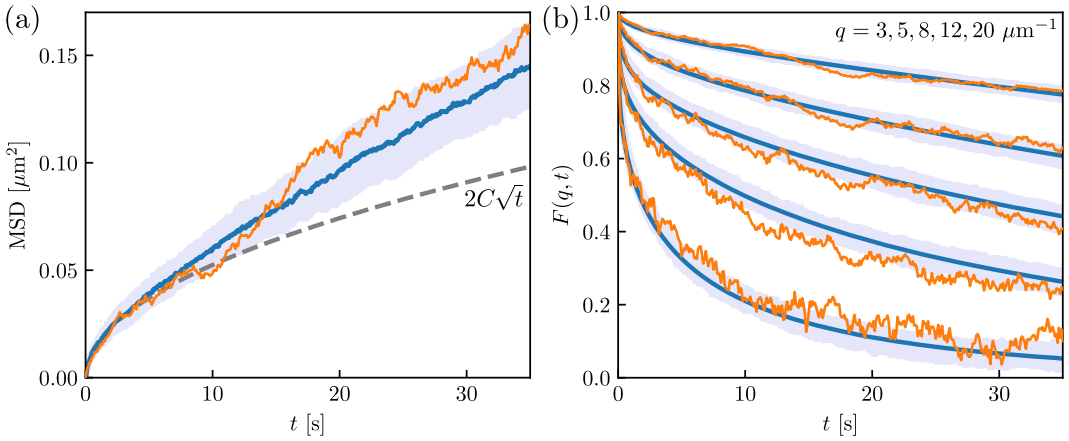

Figure 2. (a) MSD derived from the experiment (orange curve) and MSD simulated with fit parameters from (b) (blue curve with blue shaded standard deviation). The gray dashed line shows a simple subdiffusive $\sqrt{t}$-fit to the first 10 seconds, yielding $C = 0.008\,3$ μm^2 s$^{-1/2}$. (b) ISF $F(q, t)$ for (from top to bottom) $q = 3, 5, 8, 12, 20$ μm^{-1} from experiment (orange curve) and theory (blue curve) with standard deviation (blue shaded) obtained from simulations (experimental and simulation details are given in appendix D); the fitting procedure and parameters are given in the text; the range of q values was selected to capture the spatio-temporal scales in the relaxation observed experimentally, i.e. such that $F(q, t)$ spans the full range of values.

where erfcx$(x) \equiv \exp(x^2)(1 - \mathrm{erf}(x))$ and erf denotes the error function. Via equation (10) and numerical Laplace inversion this yields the two-state ISF. The theoretical ISF (blue lines) alongside the statistical uncertainty expected from a set of 400 realizations (shaded area) and the ISF determined directly from the experimental trajectories is shown in figure 2(b) for several values of q. The comparison between the corresponding MSDs is shown in figure 2(a). The theoretical fit and experimental results display a good agreement. In particular, the analysis of the ISF not only confirms the findings in reference [29] but also demonstrates the two-state FBM to be an appropriate model for the observed dynamics over a broad range of spatial and temporal scales. Notably, this spatio-temporally resolved information is inherently coarse-grained out in the analysis of the MSD. Recall that because the process is not Gaussian [29] the ISF and DSF, but not the MSD, contain the full information about the dynamics. The scattering fingerprints proposed here are thus well suited for a deeper analysis of particle-tracking experiments displaying multi-state anomalous diffusion.

3.3. Reversible dimerization with an internal mode

So far we have only considered two-state dynamics without any internal degrees of freedom. To go beyond this limitation, we consider diffusion in the presence of reversible dimerization (see figure 3(a)) captured in the mean field limit—two particles are assumed to associate with an effective rate that is independent of the particles' instantaneous position in the spirit of Smoluchowski [57, 58]. To be concrete, we consider non-interacting particles diffusing freely with a diffusion coefficient $D_1 = D$ and forming a dimer with a center-of-mass diffusion coefficient $D_2 = D/2$ and an internal harmonic vibrational relaxation mode with rate a (i.e. the internal coordinate—the distance between the associated particles—evolves as an Ornstein–Uhlenbeck process [59] or Rouse model with $N = 2$). Note that since $N > 1$ in contrast to the previous examples we here need to distinguish between coherent (i.e. equation (3)) and incoherent (i.e. equation (2)) contributions. We focus on the incoherent part (i.e. we set $\alpha = \beta$ in equation (1)) and note that the beads are equal and thus the beads $\alpha = 1$ and $\alpha = 2$ give an identical scattering contribution.

The association and dissociation rates are denoted by k_1 and k_2 respectively. Since the internal dynamics does not depend on the absolute position in space and each change of state erases all memory we can employ the result in section 2.2. In particular, this assumption neglects a possibly enhanced probability for re-association of the same pair of molecules immediately upon dissociation, which is expected to be a good approximation in well-mixed (i.e. 'stirred') systems and/or at high monomer concentrations. The opposite case, when re-association is more likely, introduces at least one more time scale in to the kinetics of association, thus rendering the two-state switching process non-Markovian. For the sake of simplicity we stick to the Markovian scenario.

The Fourier–Laplace transforms of the joint density to observe a displacement $\vec{r}$ in a time t in the respective state 1 prior to switching, $\widehat{(F\psi)}_1(q, s)$, is given by equation (12) with $D_1 = D$. Conversely, introducing $s' = s + q^2D/2 + k_2$ (note that $s' = s'(q)$ depends on q) we can write $\widehat{(F\psi)}_2(q, s)$ as (for a

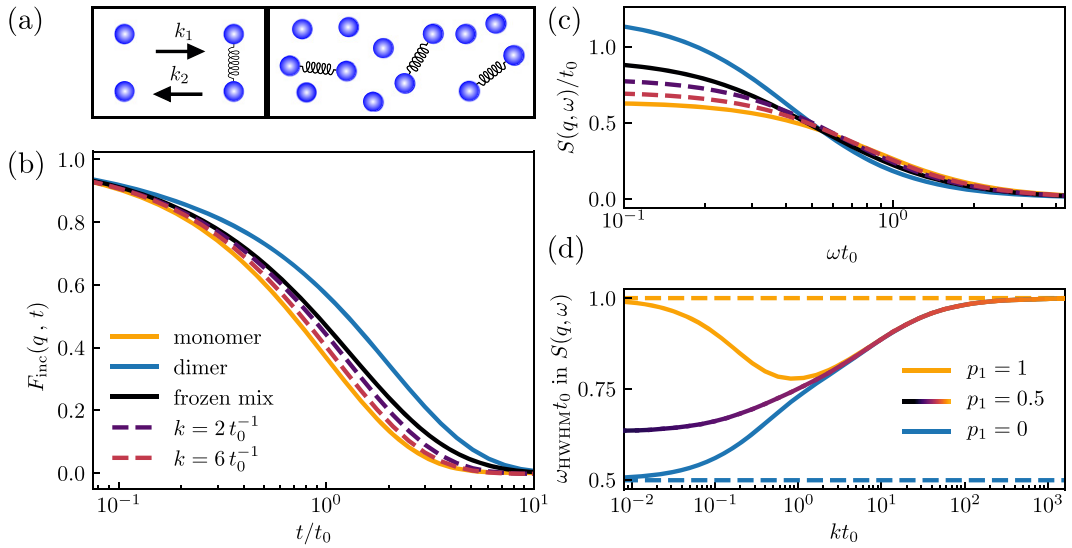

Figure 3. (a) Schematic of the dimerization process. (b) Incoherent ISF $F_{\rm inc}(q,t)$ for reversible dimerization of a two-bead (Rouse) dimer with $k = k_1 = k_2$ evolving from an equilibrium occupation $p_1 = p_2 = 0.5$ and time t measured in units of $t_0 = 1/Dq^2$. The limit for $k \to 0$ is the frozen mix (black curve) and for $k \to \infty$ the ISF approaches the ISF of a monomer without dimerization (yellow curve) since the unbinding occurs before the internal mode enters the dynamics. For the explicit derivation of this limit see appendix E. (c) DSFs corresponding to (a). (d) HWHMs of the DSF from (c) are shown along with the HWHMs of the blue and yellow curves in (c) (dashed lines). The HWHMs for initial occupation $p_1 = 0$ and $p_1 = 1$ are also shown (blue and yellow lines).

derivation see appendix E)

$$\widehat{(F\psi)}_2(q,s') = \frac{1}{s'}\,\mathrm{e}^{-q^2D/2a}\left(q^4D^2/4a^2\right)^{s'/a} M\left(\frac{s'}{a}, \frac{s'+1}{a}, \frac{q^2D}{2a}\right)$$
$$= \mathrm{e}^{-q^2D/2a}\sum_{n=0}^{\infty}\frac{(q^2D/2a)^n}{n!}\,\frac{1}{s'+na}, \tag{19}$$

where $M(a,b,z)$ denotes Kummer's confluent hypergeometric function [60]. Using $\widehat{(F\psi)}_1(\vec{q},s)$ and $\widehat{(F\psi)}_2(\vec{q},s')$ in equation (10) we find the Laplace image of the incoherent ISF and, via equation (11), also the incoherent DSF, where we recall that here the coherent and incoherent contribution do not coincide. The ISF may in principle be obtained by analytical inversion of the Laplace transform. For the sake of simplicity we here perform the inversion numerically with the fixed Talbot method.

The results for the incoherent ISF for the two-state dynamics with $k_1 = k_2 = k$ alongside the frozen mixture and dynamics in the individual pure states, all evolving from an equilibrium initial condition, are shown in figure 3(b). The corresponding DSF is depicted in figure 3(c) and the comparison is further clarified by means of the HWHM shown in figure 3(d). Altogether, one can distinguish between the different situations as long as k is not too small or too large. These results demonstrate that the scattering fingerprints proposed here may be a valuable tool for analyzing two-state dynamics also in the presence of internal motions.

3.4. Two-state dynamics with internal structural motions—protein (un)folding

A generalization of the preceding results to two-state dynamics in the presence of some general internal structural relaxation, such as, for example, in the case of cyclization of polymers, and the reversible (un)folding or association of proteins, to name but a few, is much more difficult. In particular, when the change of state does not erase all memory such that the propagation within each sojourn depends on the internal configuration just before the switch, the results of section 2.2 cannot be applied. Such a situation naturally arises in systems with internal (e.g. conformational) dynamics in absence of a complete time-scale separation, i.e. when at the time of the jump the internal degrees of freedom have not yet completely relaxed from their initial condition or the condition immediately after the preceding change of channel, respectively. If one is to nevertheless apply a version of the theory developed here, additional simplifying assumptions are required. In particular, we must assume that the switching rate is independent of the instantaneous structural state in either dynamical state. Even in this case the switching between states at any instance occurs from a distribution of structures that set the initial conditions for the relaxation following

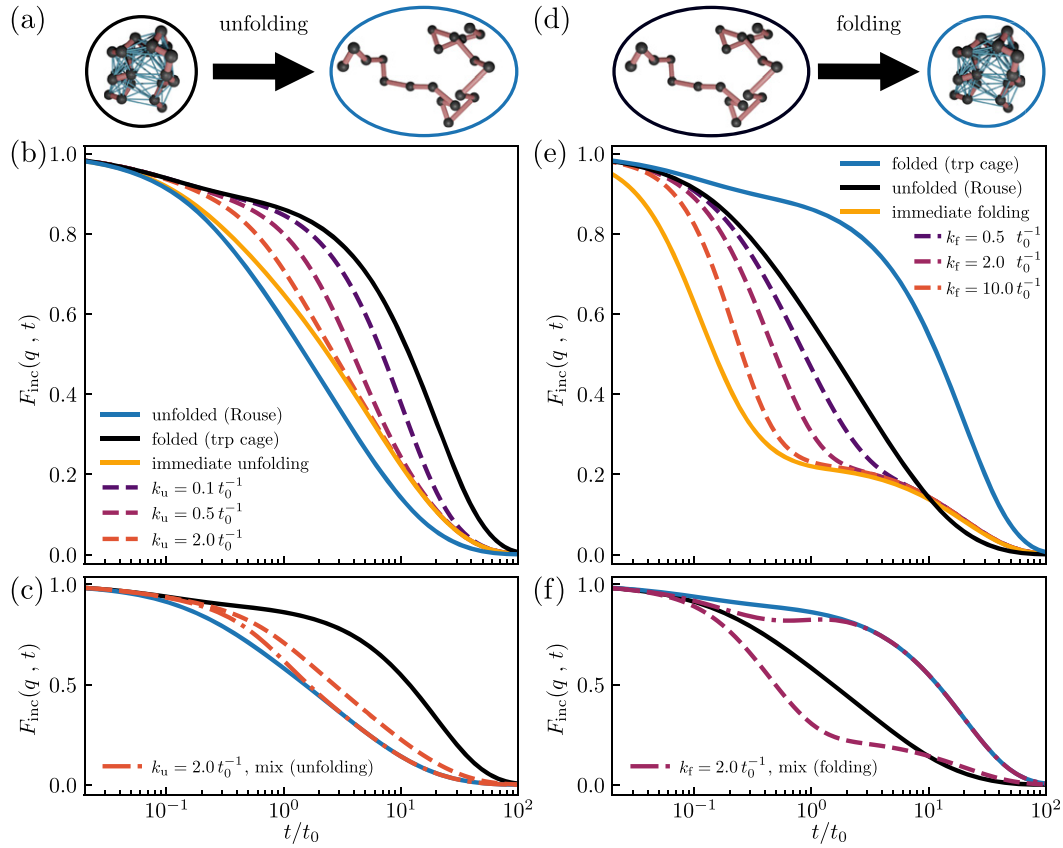

Figure 4. (a) Schematic of the Gaussian network model for the Trp-cage miniprotein construct TC5b (PDB: 1L2Y) and its unfolding to a Rouse chain ($N = 20$). (b) Incoherent ISF $F_{\rm inc}(q, t)$ for the (non-reversible) unfolding process with time measured in units of $t_0 = 1/Dq^2$ and a ratio of spring and friction constant of $k/\xi = t_0^{-1}$. The dashed lines denotes various unfolding rates $k_{\rm u}$, and the yellow curve, the 'immediate unfolding' limit, is obtained by setting $\tau = 0$ in equation (22). Also depicted are the $F_{\rm inc}(q, t)$ of the respective relaxation processes of the folded protein (black line) and the Rouse chain (blue line). Time is expressed in standard dimensionless Rouse units (see e.g. [64]). (c) Comparison of the unfolding process (dashed line) with the time-dependent 'mix' (dash-dotted line) which corresponds to the superposition of the ISF of the Rouse chain and the protein weighted by the respective time-dependent occupation of the state. (d)–(f) As in (a)–(c) but for the converse folding process.

the jump. Further, as long as the dynamical states have substantially different equilibrium structures, the ISF is expected to depend qualitatively on q (i.e. large and intermediate scale motions are expected to differ in contrast to individual bond vibrations at large q). In full generality this corresponds to a highly non-trivial problem. To render the general problem analytically tractable one may, for example, inspect the limit of slow jumps that corresponds to the switching between two equilibrium populations of internal structures. However, this limit is rather uninteresting as the state switching is too slow to mix the dynamics of the individual states, i.e. deviations form a 'frozen mix' are small. However, it is easy to instead look at the two-state dynamics with unidirectional/irreversible jumps evolving from a pure state (i.e. from either of the states). A neat and experimentally interesting problem is the denaturant-driven unfolding [61, 62] or folding [63] of proteins. To this end we analyze the irreversible unfolding/folding of the small 20-residue Trp-cage protein construct TC5b into/from a Rouse chain ($N = 20$). That is, we consider a sample initially prepared in the folded state that unfolds with rate $k_{\rm u}$ (figure 4(a)), and an initially unfolded (Rouse chain) state folding with a rate $k_{\rm f}$, respectively (figure 4(d)).

A Gaussian elastic network model [64, 65] of TCPb in the folded state was constructed from the Protein Data Bank (PDB entry: 1L2Y) using the ProDy software [66], yielding a Kirchoff matrix $A^{\rm f}$ with dimensional non-zero entries that are integer multiples of k/ξ where k and ξ are the spring and friction constant, respectively. Conversely, Rouse chain dynamics with connectivity matrix $A^{\rm u}$ [67] were assumed in the unfolded state. $A^{\rm f}$ and $A^{\rm u}$ are given explicitly in appendix F. For simplicity, in both cases the diffusion matrix is supposed to be equal and diagonal (isotropic) with diffusion coefficient $D = k_{\rm B}T/\xi$ for each individual bead. A schematic of the bead-spring model is shown in figures 4(a) and (d).

Introducing the $3N$-dimensional vector of beads' positions $\mathbf{R} \equiv \{\vec{R}^{\alpha}\}_{\alpha=1,\ldots,N}$ the equations of motion in each state follow a $3N$-dimensional Ornstein–Uhlenbeck process with positive semi-definite drift matrix $A^{\rm f/u}$, i.e. $\mathrm{d}\mathbf{R}_t = -A^{\rm f/u}\mathbf{R}_t\,\mathrm{d}t + \sqrt{2D}\,\mathrm{d}\mathbf{W}_t$ in the respective state f and u, where $\mathbf{W}$ denotes a $3N$ dimensional vector whose entries are statistically independent Wiener processes W_t. This process describes the

overdamped thermal motion of beads connected by Hookean springs with zero rest length. The analysis is most easily carried out in the respective normal coordinates $\mathbf{X}^{\mathrm{f/u}} = (Q^{\mathrm{f/u}})^{\mathrm{T}}\mathbf{R}$ with $(Q^{\mathrm{f/u}})^{\mathrm{T}}A^{\mathrm{f/u}}Q^{\mathrm{f/u}} = \mathrm{diag}\,(a_\alpha^{\mathrm{f/u}})_{\alpha=1,\ldots,N}$. For details see appendix F. We choose $\alpha = 1$ to represent the centre-of-mass mode. The center-of-mass diffusion coefficient is given by $D_{\mathrm{COM}} = D/N$ and within this model does not depend on the conformation of the protein. For all but the center-of-mass mode the equilibrium probability density function is Gaussian with zero mean and variance $V_{\mathrm{f/u}}^{\alpha}$.

To illustrate the theory it suffices to consider the folding-process alone. Let us consider the propagation in the unfolded state u evolving from the Rouse chain equilibrium distribution. We are interested in the $\alpha\beta$-component of the ISF of the folding process, $F^{\alpha\beta}(\vec{q},t)$, assuming no or a single jump occurring at time τ with $0 < \tau < t$, where τ is exponentially distributed with rate k. Let $F_{\mathrm{u}}^{\alpha\beta}(\vec{q},t)$ be the ISF of the pure unfolded state (Rouse) dynamics. As we have excluded jumps back to the folded state it is obvious that $F^{\alpha\beta}(\vec{q},t)$ corresponds to $F_{\mathrm{u}}^{\alpha\beta}(\vec{q},t)$ weighted by the probability e^{-kt} that no jump has occurred until time t, and a contribution of the folding. The latter corresponds to the dynamics in the folded state starting with a jump at the time τ and evolving from the equilibrium distribution of the unfolded (Rouse chain) state, $F_{\mathrm{u}\to\mathrm{f}}^{\alpha\beta}(\vec{q},t;\tau)$, averaged over the exponentially distributed jumping times[5], i.e.

$$F^{\alpha\beta}(\vec{q},t) = \mathrm{e}^{-kt}F_{\mathrm{u}}^{\alpha\beta}(\vec{q},t) + \int_0^t \mathrm{d}\tau\, k\,\mathrm{e}^{-k\tau}F_{\mathrm{u}\to\mathrm{f}}^{\alpha\beta}(\vec{q},t;\tau). \tag{20}$$

Since the Ornstein–Uhlenbeck process with a Gaussian initial condition is a Gaussian process, $F_{\mathrm{u}}^{\alpha\beta}(\vec{q},t)$ and $F_{\mathrm{u}\to\mathrm{f}}^{\alpha\beta}(\vec{q},t;\tau)$ are characteristic functions (see e.g. equation (4)) of zero mean Gaussian displacements and thus simply equal to $\exp[-q^2\langle(\vec{R}_t^{\alpha} - \vec{R}_0^{\beta})^2\rangle_{\mathrm{u}/\mathrm{u}\overset{\tau}{\to}\mathrm{f}}/6]$, see appendix F. Via normal mode analysis (see, e.g. [68]) we show in appendix F that the displacement vectors $\langle(\vec{R}_t^{\alpha} - \vec{R}_0^{\beta})^2\rangle_{\mathrm{u}/\mathrm{u}\overset{\tau}{\to}\mathrm{f}}$ obey

$$\left\langle\left(\vec{R}_t^{\alpha} - \vec{R}_0^{\beta}\right)^2\right\rangle_{\mathrm{u}} = 6D_{\mathrm{COM}}t + \sum_{\gamma=2}^{N} V_{\mathrm{u}}^{\gamma}\left[(Q_{\alpha\gamma}^{\mathrm{u}})^2 + (Q_{\beta\gamma}^{\mathrm{u}})^2 - 2Q_{\alpha\gamma}^{\mathrm{u}}Q_{\beta\gamma}^{\mathrm{u}}\,\mathrm{e}^{-a_\gamma^{\mathrm{u}}t}\right], \tag{21}$$

when the Rouse polymer does not fold until t, whereas in the case that folding occurs at a fixed time τ we find, introducing the notation $Q^{\mathrm{u}\to\mathrm{f}} = (Q^{\mathrm{f}})^{\mathrm{T}}Q^{\mathrm{u}}$ (s.t. analogous to $\mathbf{R}_t = Q^{\mathrm{f/u}}\mathbf{X}_t^{\mathrm{f/u}}$ we have $\mathbf{X}_t^{\mathrm{f}} = Q^{\mathrm{u}\to\mathrm{f}}\mathbf{X}_t^{\mathrm{u}}$),

$$\begin{aligned}\left\langle\left(\vec{R}_t^{\alpha} - \vec{R}_0^{\beta}\right)^2\right\rangle_{\mathrm{u}\overset{\tau}{\to}\mathrm{f}} &= 6D_{\mathrm{COM}}t + \sum_{\gamma=2}^{N}(Q_{\beta\gamma}^{\mathrm{u}})^2V_{\mathrm{u}}^{\gamma} + \sum_{\gamma=2}^{N}(Q_{\alpha\gamma}^{\mathrm{f}})^2V_{\mathrm{f}}^{\gamma}\left[1 - \mathrm{e}^{-2a_\gamma^{\mathrm{f}}(t-\tau)}\right]\\ &\quad + \sum_{\omega=2}^{N}V_{\mathrm{u}}^{\omega}\left[\sum_{\gamma=2}^{N}Q_{\alpha\gamma}^{\mathrm{f}}Q_{\gamma\omega}^{\mathrm{u}\to\mathrm{f}}\,\mathrm{e}^{-a_\gamma^{\mathrm{f}}(t-\tau)}\right]^2 - 2\sum_{\omega,\gamma=2}^{N}Q_{\alpha\omega}^{\mathrm{f}}Q_{\omega\gamma}^{\mathrm{u}\to\mathrm{f}}Q_{\beta\gamma}^{\mathrm{u}}V_{\mathrm{u}}^{\gamma}\,\mathrm{e}^{-a_\omega^{\mathrm{f}}(t-\tau)-a_\gamma^{\mathrm{u}}\tau}.\end{aligned} \tag{22}$$

The converse unfolding process is obtained by interchanging $\mathrm{u} \leftrightarrow \mathrm{f}$. Plugging equations (21) and (22) into equation (20) and performing a numerical integration over τ yields the result for $F^{\alpha\beta}(\vec{q},t)$. Summations over α, β deliver the (in)coherent ISF, see equations (2) and (3).

In figures 4(b), (c), (e) and (f) we show, respectively, the incoherent part of the ISF for various unfolding and folding rates. The limit of large (un)folding rates is given by setting $\tau = 0$ in the Gaussian ISF for the displacement vector from equation (22). The discrepancy between the immediate (un)folding limit and dynamics in the target (un)folded structure (yellow and blue curves in figures 4(b) and (e), respectively) is solely caused by the different initial conditions whereas the propagator is in both cases identical. Notably, this difference is small in the unfolding process but substantial during folding. Several additional remarks are in order. The ISF reflects dynamics on a given spatial (i.e. q-value) scale and thus the projections onto different relaxation eigenmodes play an important role (see also e.g. [69]). The aforementioned discrepancies are a result of initial conditions (and starting conditions upon a jump) that put more weight onto faster relaxation modes rendering the decay of the ISF faster (this idea is corroborated in figure 4(e)). Note that relaxation in the folded state is faster than in the unfolded and yet the ISF in the folded state in figure 4(b) decays the slowest. This means that said differences are not only caused by a shorter relaxation time (i.e. larger principal eigenvalue of the underlying generator).

For a comparison, in figures 4(c) and (f) we also show the incoherent ISF for the time-dependent mix, $F_{\mathrm{u/f}}^{\mathrm{mix}}(\vec{q},t) \equiv \mathrm{e}^{-k_{\mathrm{u/f}}t}\sum_\alpha F_{\mathrm{f/u}}^{\alpha\alpha}(\vec{q},t) + (1 - \mathrm{e}^{-k_{\mathrm{u/f}}t})\sum_\alpha F_{\mathrm{u/f}}^{\alpha\alpha}(\vec{q},t)$, which represents the trivial time-dependent approximation of the ISF for the unfolding and folding processes, respectively. In the case of unfolding the (trivial) mix displays qualitative differences with respect to exact the two-state (single jump) solution but

[5] It is straightforward to include non-exponential jumping-time distributions.

the quantitative differences are rather small (see figure 4(c)). Conversely, in the case of folding the mix-approximation $F_{\rm f}^{\rm mix}$ fails completely (see figure 4(f)) due to the striking dependence on the initial condition that is not included in the (trivial) mix. This clearly illustrates the importance of considering jump dynamics explicitly.

Overall, our results suggest that scattering fingerprints may be a useful observable to probe two-state dynamics even in the presence of non-trivial internal structural relaxation, such as e.g. probed in references [61–63]. A systematic study of the relaxation at various values of the dimensionless quantities $k_{\rm u,f}t_0$ and t_0k/ξ may provide further details, which is, however, beyond the scope of the present proof-of-principle investigation. Moreover, one can easily generalize the model to include internal friction [70] or hydrodynamic interactions in the spirit of the Zimm model [71]. Finally, one may also consider springs with a non-zero rest length in the context of so-called Gaussian models (see e.g. [64]).

4. Conclusion

Scattering experiments on polymerizing chains revealed pronounced signatures of multi-state dynamics [51]. Moreover, observations of particle transport in complex environments such as the interior of living cells often reveal a non-Fickian (or non-Brownian) character that may also display multi-state characteristics [16–24, 27–29]. Reliably distinguishing between single- and multi-state dynamics remains challenging. To complement the existing approaches we addressed scattering fingerprints of two-state dynamics—the ISF and structure factor. A combination of theory, analysis of simple model systems and of experiments in living cells revealed the potential usefulness of these scattering fingerprints.

We addressed both, inert tracer-particle dynamics as well as dynamics in systems with an internal structure and dynamics. In all examples the ISF decays faster for increasing switching rates, which is consistent with the idea of an additional relaxation channel enabling a faster decay [72, 73]. However, this view contradicts the multi-state dynamics in [51], where an empirical ansatz assumed a mode-scission that leads to a slower decay of the ISF.

The present results can be extended to incorporate non-Markovian (i.e. non-exponential) waiting time statistics in the respective states (see e.g. [74–76]), and may be relevant and useful for digital Fourier microscopy (DDM and FICS) experiments on complex particulate systems, as well as neutron (incl. spin-echo) and x-ray scattering probing structural and dynamical properties of macromolecules, as soon as the dynamics displays two-state transport.

Acknowledgments

We thank Maximilian Vossel for preparing figures 4(a) and (d), and Adal Sabri for providing the data from reference [29]. The financial support from the Studienstiftung des Deutschen Volkes (to CD), and the German Research Foundation (DFG) through the *Emmy Noether Program* '*GO* 2762/1-1' (to AG) is gratefully acknowledged.

Data availability statement

The data that support the findings of this study are available upon reasonable request from the authors.

Appendix A. Derivation of equation (10)

Here we derive equation (10) for the Laplace-transformed ISF of the two-state dynamics following the reference [54]. For this approach to hold, memory in the process has to be erased at the instance of the jump and the instantaneous position at the jump must not influence the probability of subsequent displacements. These assumptions can arise as a consequence of translation invariance of the dynamics in single dynamical states, as in the examples of two-state diffusion and FBM. However, translation invariance is not a necessary condition, as e.g. in the case of the process studied in [54].

For a Markov jump process the probability to remain in a state for a time t is given by $\psi_j(t) = {\rm e}^{-k_jt}$. Recall that the van Hove functions $G_j(\vec{r},t) = \langle\delta(\vec{r}(t)-\vec{r}(0)-\vec{r})\rangle_j$ in the two individual states $j = 1, 2$ give the probability of performing a displacement $\vec{r}$ in time t. We now set $N = 1$ and omit the indices α, β compared to equation (1). For $N > 1$ the assumption of memory erasure is rarely satisfied as a result of internal dynamics (see e.g. section 3.4). If it is satisfied also for $N > 1$, as e.g. in section 3.3 where $N = 2$, then for $\alpha = \beta$ the approach does not change and equation (10) gives an equation for $\widehat{F}^{\alpha\alpha}(\vec{q},s)$ that can

subsequently be summed over α. For $\alpha \neq \beta$ only the displacement probability prior to the first memory erasure is different, and the approach below may applied with slight modifications.

Following [54], we write down the probability $\mathcal{P}_n(\vec{r},t)$ of a displacement $\vec{r}$ in time t conditioned on a fixed number of n jumps for $n = 0, 1, 2$, given that we start in state 1 at $t = 0$, and adopting the notation $G_j(\vec{r},t)\psi_j(t) \equiv (G\psi)_j(\vec{r},t)$,

$$\begin{aligned}
\mathcal{P}_0(\vec{r},t) &= (G\psi)_1(\vec{r},t)\\
\mathcal{P}_1(\vec{r},t) &= \int \mathrm{d}^3 r_1 \int_0^t \mathrm{d}t_1 k_1 (G\psi)_1(\vec{r}_1,t_1)(G\psi)_2(\vec{r}-\vec{r}_1,t-t_1)\\
\mathcal{P}_2(\vec{r},t) &= \int \mathrm{d}^3 r_1 \int \mathrm{d}^3 r_2 \int_0^t \mathrm{d}t_2 \int_0^{t_2} \mathrm{d}t_1\, k_1 (G\psi)_1(\vec{r}_1,t_1) k_2 (G\psi)_2(\vec{r}_2-\vec{r}_1,t_2-t_1)\times\\
&\qquad (G\psi)_1(\vec{r}-\vec{r}_2,t-t_2). \qquad \text{(A.1)}
\end{aligned}$$

By the assumption of independence of the position at the time of the jump, this has a convolution structure in space and we Fourier transform $\vec{r} \to \vec{q}$, $\mathcal{P} \to \widetilde{\mathcal{P}}$ to obtain, e.g. for $n = 2$,

$$\widetilde{\mathcal{P}}_2(\vec{q},t) = \int_0^t \mathrm{d}t_2 \int_0^{t_2} \mathrm{d}t_1\, k_1 \widetilde{(G\psi)}_1(\vec{q},t_1) k_2 \widetilde{(G\psi)}_2(\vec{q},t_2-t_1) \widetilde{(G\psi)}_1(\vec{q},t-t_2). \qquad \text{(A.2)}$$

Recalling that the ISF $F(\vec{q},t)$ is the Fourier transform of the van Hove function $G(\vec{r},t)$, and noting the convolution structure (defined as $[f*g](t) \equiv \int_0^t \mathrm{d}t' f(t') g(t-t')$) in time, we have

$$\begin{aligned}
\widetilde{\mathcal{P}}_2(\vec{q},t) &= \int_0^t \mathrm{d}t_2 \int_0^{t_2} \mathrm{d}t_1\, k_1 (F\psi)_1(\vec{q},t_1) k_2 (F\psi)_2(\vec{q},t_2-t_1)(F\psi)_1(\vec{q},t-t_2)\\
&= k_1 k_2 \int_0^t \mathrm{d}t_2 (F\psi)_1(\vec{q},t-t_2) \left[(F\psi)_1(\vec{q},\cdot) * (F\psi)_2(\vec{q},\cdot)\right](t_2)\\
&= k_1 k_2 \left[(F\psi)_1 * (F\psi)_1 * (F\psi)_2\right](\vec{q},t). \qquad \text{(A.3)}
\end{aligned}$$

Taking the Laplace transform $t \to s$ gives

$$\widehat{\mathcal{P}}_2(\vec{q},s) = k_1 k_2 \left[\widehat{(F\psi)}_1(\vec{q},s)\right]^2 \widehat{(F\psi)}_2(\vec{q},s). \qquad \text{(A.4)}$$

This generalizes to all even $n = 2m$ and odd $n = 2m+1$ terms as

$$\begin{aligned}
\widehat{\mathcal{P}}_{2m+1}(\vec{q},s) &= k_1^{m+1} k_2^m \left[\widehat{(F\psi)}_1(\vec{q},s)\right]^{m+1} \left[\widehat{(F\psi)}_2(\vec{q},s)\right]^{m+1},\\
\widehat{\mathcal{P}}_{2m}(\vec{q},s) &= k_1^m k_2^m \left[\widehat{(F\psi)}_1(\vec{q},s)\right]^{m+1} \left[\widehat{(F\psi)}_2(\vec{q},s)\right]^{m}. \qquad \text{(A.5)}
\end{aligned}$$

The Fourier–Laplace transform of the probability of a displacement in the two-state dynamics that by the assumption of memory erasure and independence of the jump position is the Laplace-transformed ISF $\widehat{F}(\vec{q},s)$, is then given by the geometric series

$$\begin{aligned}
\widehat{F}(\vec{q},s) &= \sum_{n=0}^{\infty} \widehat{\mathcal{P}}_n(\vec{q},s)\\
&= \sum_{m=0}^{\infty} \left[\widehat{\mathcal{P}}_{2m}(\vec{q},s) + \widehat{\mathcal{P}}_{2m+1}(\vec{q},s)\right]\\
&= \widehat{(F\psi)}_1(\vec{q},s) \left[1 + k_1 \widehat{(F\psi)}_2(\vec{q},s)\right] \sum_{m=0}^{\infty} \left[k_1 k_2 \widehat{(F\psi)}_1(\vec{q},s) \widehat{(F\psi)}_2(\vec{q},s)\right]^m\\
&= \widehat{(F\psi)}_1(\vec{q},s) \frac{1 + k_1 \widehat{(F\psi)}_2(\vec{q},s)}{1 - k_1 k_2 \widehat{(F\psi)}_1(\vec{q},s) \widehat{(F\psi)}_2(\vec{q},s)}. \qquad \text{(A.6)}
\end{aligned}$$

Assuming initial occupations p_j of the two states (not necessarily $p_j = p_j^{\mathrm{eq}}$), and repeating the same treatment for starting conditions in state 2 yields the result equation (10),

$$\widehat{F}(\vec{q},s) = \frac{p_1 \widehat{(F\psi)}_1 \left[1 + k_1 \widehat{(F\psi)}_2\right] + p_2 \widehat{(F\psi)}_2 \left[1 + k_2 \widehat{(F\psi)}_1\right]}{1 - k_1 k_2 \widehat{(F\psi)}_1 \widehat{(F\psi)}_2}. \qquad \text{(A.7)}$$

Appendix B. Two-state diffusion in the slow- and fast-switching limit

Here we consider the slow-switching limit of two-state diffusion in section 3.1, that is, the limit of small switching rates, $k_1 + k_2 \ll q^2 D_{1,2}$. In this limit, equation (14) gives $\mu_+ \approx q^2 D_1$ and $\mu_- \approx q^2 D_2$. Since $p_2 = 1 - p_1$ we obtain $\phi(q) \approx p_2$ and thus equation (16) in the slow-switching limit results in the frozen mixture,

$$F(q,t) \approx p_1\, \mathrm{e}^{-q^2 D_1 t} + p_2\, \mathrm{e}^{-q^2 D_2 t} = F_{\mathrm{mix}}(q,t). \tag{B.1}$$

Now consider the fast-switching limit, $k_1 + k_2 \gg q^2 D_{1,2}$ with a finite ratio $k_1/k_2 = p_2^{\mathrm{eq}}/p_1^{\mathrm{eq}}$ (when this ratio is zero or infinite we recover single-state dynamics). We introduce the notation $k \equiv (k_1 + k_2)/2$, $\kappa \equiv (k_1 - k_2)/2$, $\bar{d} \equiv q^2(D_1 + D_2)/2$ and $\Delta \equiv q^2(D_2 - D_1)/2$. Then equation (14) reads

$$\begin{aligned} \mu_{1,2} &= \bar{d} + k \pm \sqrt{(\Delta + \kappa)^2 + k^2 - \kappa^2} \\ &= \bar{d} + k \pm \sqrt{\Delta^2 + 2\Delta\kappa + k^2}. \end{aligned} \tag{B.2}$$

In the limit of fast jumps $k \gg \bar{d} > |\Delta|$ we have

$$\begin{aligned} \mu_{1,2} &= \bar{d} + k \pm k\sqrt{1 + \frac{2\Delta\kappa + \Delta^2}{k^2}} \approx \bar{d} + k\left[1 \pm \left(1 + \frac{2\Delta\kappa + \Delta^2}{2k^2}\right)\right], \\ \mu_1 &\approx \bar{d} - \frac{2\Delta\kappa + \Delta^2}{2k} \approx \bar{d} - \frac{\kappa}{k}\Delta, \quad \mu_2 \approx \bar{d} + 2k + \frac{2\Delta\kappa + \Delta^2}{2k} \approx 2k \overset{k\to\infty}{\longrightarrow} \infty. \end{aligned} \tag{B.3}$$

Using equation (7), we have $k_1 = 2p_2^{\mathrm{eq}} k$ and $k_2 = 2p_1^{\mathrm{eq}} k$ and arrive at

$$\mu_1 \approx \bar{d} - \frac{\kappa}{k}\Delta = \bar{d} + \Delta\frac{p_2^{\mathrm{eq}} - p_1^{\mathrm{eq}}}{p_2^{\mathrm{eq}} + p_1^{\mathrm{eq}}} = q^2(p_1^{\mathrm{eq}} D_1 + p_2^{\mathrm{eq}} D_2). \tag{B.4}$$

Thus, the exponential with rate μ_1 in equation (16) gives an exponential with effective diffusion constant $D_{\mathrm{eff}} \equiv p_1^{\mathrm{eq}} D_1 + p_2^{\mathrm{eq}} D_2$, while the second exponential with rate $\mu_2 \approx 2k$ immediately decays in the limit of large k. This proves that for large k the ISF of two-state diffusion approaches effective diffusion, i.e. in figure 1(a) the dashed lines approach the yellow line.

Appendix C. Laplace transforms for fractional Brownian motion

We consider FBM in d dimensions with MSD

$$\left\langle [\vec{r}(t) - \vec{r}(0)]^2 \right\rangle = 2dC_j t^{\alpha_j}. \tag{C.1}$$

Here, the two different states are characterized by different generalized diffusion constants C_1 and C_2 and/or different 'anomalous' exponents α_1 and α_2. We still consider Markov jumps and by Gaussianity we have the Fourier-transformed displacement probabilities in a state

$$F_j(\vec{q},t)\psi_j(t) = \exp(-[q^2 C_j t^{\alpha_j} + k_j]t). \tag{C.2}$$

Assuming that each jump (i.e. change of state) erases memory the structure factor for the two-state dynamics follows from equation (10) which requires taking the Laplace transform of equation (C.2). For our purposes we consider subdiffusive FBM with $\alpha \in (0,1)$ (for $\alpha = 1$ see equation (12)). The Laplace transform of equation (C.2) can of course be performed numerically [77], and for any rational $\alpha \in (0,1)$ it can be expressed in terms of Meijer G-functions, using that for two positive integers $l < m$ [78]

$$\widehat{[\mathrm{e}^{-at^{l/m}}]}(s) = \frac{\sqrt{ml}}{s(2\pi)^{(m+l)/2-1}} G_{l,m}^{m,l}\left(\frac{a^m l^l}{m^m p^l}\,\middle|\, \begin{matrix}\Delta(l,0)\\ \Delta(m,0)\end{matrix}\right). \tag{C.3}$$

For the special case $\alpha = 0.5$ the Laplace transform of equation (C.2) follows from [78]

$$\widehat{[\mathrm{e}^{-a\sqrt{t}}]}(s) = \frac{1}{s} - \frac{a}{2}\sqrt{\frac{\pi}{s^3}}\,\mathrm{erfcx}\left(\frac{a}{2\sqrt{s}}\right), \tag{C.4}$$

where $\mathrm{erfcx}(x) = \exp(x^2)(1 - \mathrm{erf}(x))$ and erf denotes the error function, and therefore

$$\widehat{(F\psi)}_j(\vec{q},s) = \frac{1}{s + k_j} - \frac{\sqrt{\pi} q^2 C_j}{2(s + k_j)^{3/2}}\,\mathrm{erfcx}\left(\frac{q^2 C_j}{2\sqrt{s + k_j}}\right). \tag{C.5}$$

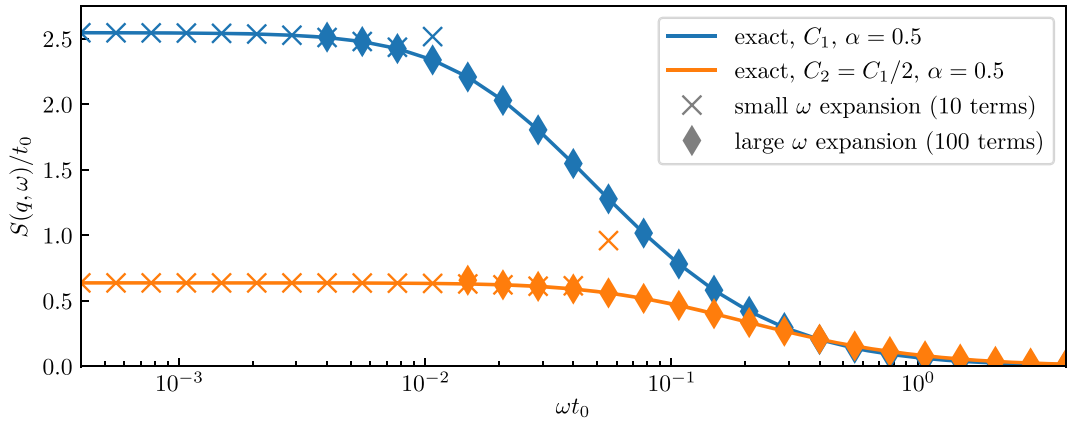

Figure C1. Illustration of the asymptotics for the DSF as introduced in equation (11). Time is measured in units of $t_0 = 1/(C_1^2 q^4)$. The large-ω series (C.6) and the small-ω expansion (C.7) together give a very good approximation to the exact DSF, i.e. the Fourier transform of equation (C.2) with $k = 0$.

Inserting $s = -\mathrm{i}\omega$ and taking the real part as in equation (17), we obtain the DSF. Numerically transforming back to the time-domain in turn yields the ISF.

For $\alpha \neq 0.5$, instead of using Meijer-G-functions or numerical solutions we can perform a series expansion [77]. We expand e^{-ct^α} around $t = 0$

$$\begin{aligned}\int_0^\infty \mathrm{e}^{-st}\,\mathrm{e}^{-ct^\alpha}\,\mathrm{d}t &= \sum_{n=0}^{\infty}\frac{(-1)^n c^n}{n!}\int_0^\infty \mathrm{e}^{-st}\,t^{n\alpha}\,\mathrm{d}\,t \\ &= \sum_{n=0}^{\infty}\frac{(-1)^n\Gamma(\alpha n+1)}{n!}c^n s^{-(\alpha n+1)},\end{aligned} \tag{C.6}$$

where the sum and integral commute since the sum is bounded by $\mathrm{e}^{-ct^\alpha},\ c > 0$ which is integrable for $\alpha < 1$. A series for the Laplace transform of equation (C.2) is obtained by shifting $s \mapsto s + k_j$ and using $c = q^2 C_j$. This approximation works particularly well for or small q, not too small s, k and $\alpha < 1$ not too close to 1.

The complementary expansion for small s reads

$$\begin{aligned}\int_0^\infty \mathrm{e}^{-st}\,\mathrm{e}^{-ct^\alpha}\,\mathrm{d}t &\approx \sum_{n=0}^{N}\frac{(-1)^n s^n}{n!}\int_0^\infty t^n\,\mathrm{e}^{-ct^\alpha}\,\mathrm{d}t \\ &= \frac{1}{\alpha}\sum_{n=0}^{N}\frac{(-1)^n}{n!}\Gamma\left(\frac{n+1}{\alpha}\right)c^{-\frac{n+1}{\alpha}}s^n.\end{aligned} \tag{C.7}$$

However, note that for $\alpha < 1$ this series is only asymptotically convergent [77], and therefore has to be truncated at some finite N to be able to swap the integration and summation. We use this expansion in the very small s regime in cases where the expansion (C.6) does not suffice.

The two asymptotic results combined yield a very good approximation as illustrated for the DSF of an FBM in figure C1 (recall that the DSF follows from the Laplace transform of equation (C.2) for $k_j = 0$ by setting $s = -\mathrm{i}\omega$ and taking the real part as in equation (11)). Combining the two expansions allows for efficient computation of $(\widehat{F\psi})(q,s)$ and $S(q,\omega)$ over the whole ω regime for general $\alpha \in (0,1)$, which in turn allows via equation (10) to deduce the two-state ISF.

Appendix D. Simulation details

The experimental data shown in figure 2 consists of 200 two-dimensional trajectories which by assuming isotropy are treated as 400 one-dimensional realizations of the two-state FBM. The experimental ISF is obtained by averaging $\mathrm{e}^{-\mathrm{i}q[r(t)-r(0)]}$ over the 400 realizations. Although the ISF of the model is deterministic, the experimental ISF obtained from a finite number of realizations fluctuates around the deterministic ISF. To estimate these fluctuations we performed simulations of $20\,000 = 500 \times 400$ two-state FBM trajectories with the parameters obtained by the fit. The standard deviation in each point of the ISF averaged over sets

of 400 trajectories is shown in figure 2. Moreover, the MSD and its fluctuations upon averaging over 400 realizations are obtained from the simulations and shown in figure 2.

Simulations were performed by drawing exponentially distributed waiting times for the state switching and simulating FBM trajectories between the switching times. The FBM simulations were performed using the Davies–Harte-algorithm [79] using the 'fbm' python package available on PyPI.

Appendix E. Details on dimerization with an internal mode

The ISF of the dimer is the characteristic function of a Gaussian with displacement given by equation (21) for $N = 2$ for which

$$A = \begin{bmatrix} 1 & -1 \\ -1 & 1 \end{bmatrix}, \qquad Q = \frac{1}{\sqrt{2}} \begin{bmatrix} 1 & -1 \\ 1 & 1 \end{bmatrix}. \tag{E.1}$$

With $D_{\mathrm{COM}} = D_2 = D/2$, $V(\infty) = 3D/a$ and $\psi_2(t) = \mathrm{e}^{-k_2 t}$ we obtain

$$\begin{aligned} (F\psi)_2(q,t) &= \exp\left[-q^2 D_2 t - k_2 t - \frac{q^2 D}{2a}\left(1 - \mathrm{e}^{-at}\right)\right] \\ &= \mathrm{e}^{-\frac{q^2 D}{2a}}\, \mathrm{e}^{-(q^2 D_2 + k_2)t}\, \exp\left(\frac{q^2 D}{2a}\, \mathrm{e}^{-at}\right), \end{aligned} \tag{E.2}$$

where for convenience we have assumed equilibrium initial conditions of the dimer.

The Laplace transform can be conveniently carried out via a series expansion (the order of summation and integration can be interchanged due to dominated convergence, i.e. since the series is bounded from above by the full expression),

$$\begin{aligned} \widehat{(F\psi)}_2(q,s) &= \mathrm{e}^{-\frac{q^2 D}{2a}} \int_0^\infty \mathrm{d}t\, \mathrm{e}^{-(s + q^2 D_2 + k_2)t}\, \exp\left(\frac{q^2 D}{2a}\, \mathrm{e}^{-at}\right) \\ &= \mathrm{e}^{-\frac{q^2 D}{2a}} \sum_{n=0}^{\infty} \frac{\left(\frac{q^2 D}{2a}\right)^n}{n!} \int_0^\infty \mathrm{d}t\, \mathrm{e}^{-(s + q^2 D_2 + k_2 + na)t} \\ &= \mathrm{e}^{-\frac{q^2 D}{2a}} \sum_{n=0}^{\infty} \frac{\left(\frac{q^2 D}{2a}\right)^n}{n!} \frac{1}{s + q^2 D_2 + k_2 + na}. \end{aligned} \tag{E.3}$$

The series expansion converges very well, especially for small q and large t (or small ω). Note that there exists a closed form expression of $\widehat{(F\psi)}_2(q,s)$ in terms Kummer's hypergeometric function [78] (or in terms of the incomplete gamma function [37]) as in equation (19).

In the limit of fast jumps $k_1, k_2 \gg q^2 D$ the time spent in a single state prior to a jump becomes very small, $at \ll 1$, for which we expand

$$\begin{aligned} (F\psi)_2(\vec{q},t) &= \mathrm{e}^{-\frac{q^2 D}{2a}}\, \mathrm{e}^{-(q^2 D_2 + k_2)t}\, \exp\left(\frac{q^2 D}{2a}\, \mathrm{e}^{-at}\right) \\ &\overset{t\to 0}{\approx} \mathrm{e}^{-\frac{q^2 D}{2a}}\, \mathrm{e}^{-(q^2 D_2 + k_2)t}\, \mathrm{e}^{\frac{q^2 D}{2a}(1-at)} \\ &= \mathrm{e}^{-(q^2 D + k_2)t} \\ &= F_1(\vec{q},t)\psi_2(t). \end{aligned} \tag{E.4}$$

Therefore, for $k_1, k_2 \gg q^2 D$ the two-state ISF converges to the simple monomer diffusion, i.e. the dashed lines approach the yellow line in figure 3(b).

Appendix F. Two-state dynamics with internal structure/dynamics—irreversible protein (un)folding

Here we derive equations (21) and (22) using normal mode analysis as introduced in section 3.4, i.e. in the normal coordinates $\mathbf{X}^{\mathrm{f/u}} = (Q^{\mathrm{f/u}})^{\mathrm{T}}\mathbf{R}$ with $(Q^{\mathrm{f/u}})^{\mathrm{T}} A^{\mathrm{f/u}} Q^{\mathrm{f/u}} = \mathrm{diag}\,(a_\alpha^{\mathrm{f/u}})_{\alpha=1,\ldots,N}$. The drift matrix $A^{\mathrm{f/u}}$ can be considered as $N \times N$-dimensional since the model assumes isotropy in all three dimensions and thus each eigenspace of the $3N \times 3N$ drift matrix is threefold degenerate. Note that $(Q^{\mathrm{f/u}})^{-1} = (Q^{\mathrm{f/u}})^{\mathrm{T}}$, and in normal coordinates (omitting index f/u) we have $\mathrm{d}\vec{X}_t^\alpha = -a_\alpha \vec{X}_t^\alpha \mathrm{d}t + \sqrt{2D}\,\mathrm{d}\vec{W}_t^\alpha$.

We choose the first mode $\alpha = 1$ to correspond to the zero eigenvalue, i.e. $a_1 = 0$ and thus $\vec{X}_t^1$ evolves as a free diffusion, capturing to the center-of-mass motion with $Q_{\alpha 1}^{\mathrm{f/u}} = N^{-1/2}$ and $D_{\mathrm{COM}} = D/N$. The position at time $t = 0$ of the center of mass cancels out in all displacements and only differences between time 0 and t enter. Thus, whenever we speak of the equilibrium initial conditions we refer to the equilibrium of modes $\vec{X}^\alpha$, $\alpha > 1$, and the initial condition of the $\vec{X}^1$-mode is irrelevant.

The $\vec{X}^\alpha$ modes with $\alpha > 1$ have $a_\alpha > 0$ and are thus described by an Ornstein–Uhlenbeck process [59], for which we obtain from the stochastic differential equation that for any $\tau \in [0, t]$

$$\mathrm{d}\left\langle \vec{X}_{t'}^\alpha \cdot \vec{X}_0^\beta \right\rangle = -a_\alpha \left\langle \vec{X}_{t'}^\alpha \cdot \vec{X}_0^\beta \right\rangle \mathrm{d}t' \quad \Rightarrow \quad \left\langle \vec{X}_t^\alpha \cdot \vec{X}_0^\beta \right\rangle = \mathrm{e}^{-a_\alpha(t-\tau)} \left\langle \vec{X}_\tau^\alpha \cdot \vec{X}_0^\beta \right\rangle, \tag{F.1}$$

and using Itô's lemma as well as the shorthand notation $V^\alpha(t) = \frac{3D}{a_\alpha}(1 - \mathrm{e}^{-2a_\alpha t})$,

$$\begin{aligned} \mathrm{d}\left\langle \vec{X}_{t'}^\alpha \cdot \vec{X}_{t'}^\beta \right\rangle &= \left\langle \mathrm{d}\vec{X}_{t'}^\alpha \cdot \vec{X}_{t'}^\beta \right\rangle + \left\langle \vec{X}_{t'}^\alpha \cdot \mathrm{d}\vec{X}_{t'}^\beta \right\rangle + \frac{1}{2}\left\langle \mathrm{d}\vec{X}_{t'}^\alpha \cdot \mathrm{d}\vec{X}_{t'}^\beta \right\rangle \\ &= -(a_\alpha + a_\beta)\left\langle \vec{X}_{t'}^\alpha \cdot \vec{X}_{t'}^\beta \right\rangle \mathrm{d}t' + 3D\delta_{\alpha\beta}\,\mathrm{d}t' \\ \Rightarrow \quad \left\langle \vec{X}_t^\alpha \cdot \vec{X}_t^\beta \right\rangle &= \left\langle \vec{X}_\tau^\alpha \cdot \vec{X}_\tau^\beta \right\rangle \mathrm{e}^{-(a_\alpha + a_\beta)(t-\tau)} + \delta_{\alpha\beta} V^\alpha(t-\tau), \end{aligned} \tag{F.2}$$

and thus for equilibrium initial conditions $\left\langle \vec{X}_t^\alpha \cdot \vec{X}_t^\beta \right\rangle_{\mathrm{eq}} = \delta_{\alpha\beta} V^\alpha(\infty) \equiv \delta_{\alpha\beta} V^\alpha$.

Since the Ornstein–Uhlenbeck process with a Gaussian initial condition is a Gaussian process, $F_{\mathrm{u}}^{\alpha\beta}(\vec{q}, t)$ and $F_{\mathrm{u}\to\mathrm{f}}^{\alpha\beta}(\vec{q}, t; \tau)$ are characteristic functions, of zero mean Gaussian displacement vectors. For any real Gaussian stochastic process $Y_t, 0 \leqslant t \leqslant T$ the characteristic function of the joint probability distribution of the random variables $Y_{t_1} \ldots Y_{t_n}$ with $0 \leqslant t_1 \ldots t_n \leqslant T$ $(n < \infty)$ is given by $\phi(q_1 \ldots q_n) = \exp(\mathrm{i}\sum_{k=1}^n \langle Y_{t_k}\rangle q_k - \sum_{k,l=1}^n \langle [Y_{t_k} - \langle Y_{t_k}\rangle][Y_{t_l} - \langle Y_{t_l}\rangle]\rangle q_k q_l/2)$, which naturally generalizes to d-dimensional Gaussian stochastic process with vector values $\vec{Y}_t = (Y_t^1, \ldots, Y_t^d)$ $(d < \infty)$ [80]. In our case we have $\vec{Y}_{t_k} = \vec{R}_{t_k}^\alpha - \vec{R}_{t_{k-1}}^\beta$, $n = 1$, and $\langle \vec{Y}_{t_k}\rangle = 0$, $\forall\ t_k$ because all involved Gaussian distributions are centered at zero, and the additional factor of $1/3$ in $q^2/6$ is due to isotropy. Therefore, $F_{\mathrm{u/u}\overset{\tau}{\to}\mathrm{f}}^{\alpha\beta}(\vec{q}, t) = \exp[-q^2\langle(\vec{R}_t^\alpha - \vec{R}_0^\beta)^2\rangle_{\mathrm{u/u}\overset{\tau}{\to}\mathrm{f}}/6]$ and we only need to compute the squared displacements $\langle(\vec{R}_t^\alpha - \vec{R}_0^\beta)^2\rangle_{\mathrm{u/u}\overset{\tau}{\to}\mathrm{f}}$ to obtain the ISFs.

We first consider the single-state process, say in the unfolded state u, with equilibrium initial conditions and now derive the result equation (21). Using normal coordinates $\mathbf{R} = Q^{\mathrm{u}}\mathbf{X}^{\mathrm{u}}$ (from now on omit index u in $\mathbf{X}^{\mathrm{u}}$), the independence of modes, and that the mean value vanishes, we obtain

$$\begin{aligned} \left\langle \left[\vec{R}_t^\alpha - \vec{R}_0^\beta\right]^2 \right\rangle_{\mathrm{u}} &= \left\langle \left[\sum_{\gamma=1}^N \left(Q_{\alpha\gamma}^{\mathrm{u}}\vec{X}_t^\gamma - Q_{\beta\gamma}^{\mathrm{u}}\vec{X}_0^\gamma\right)\right]^2 \right\rangle_{\mathrm{u}} \\ &= \sum_{\gamma=1}^N \left\langle \left(Q_{\alpha\gamma}^{\mathrm{u}}\vec{X}_t^\gamma - Q_{\beta\gamma}^{\mathrm{u}}\vec{X}_0^\gamma\right)^2 \right\rangle_{\mathrm{u}}. \end{aligned} \tag{F.3}$$

The center-of-mass motion with $D_{\mathrm{COM}} = D/N$ is obtained from $Q_{\alpha 1}^{\mathrm{u}} = Q_{\beta 1}^{\mathrm{u}} = N^{-1/2}$. Using equations (F.1) and (F.2) we directly obtain the result equation (21),

$$\left\langle \left(\vec{R}_t^\alpha - \vec{R}_0^\beta\right)^2 \right\rangle_{\mathrm{u}} = 6D_{\mathrm{COM}}t + \sum_{\gamma=2}^N V_{\mathrm{u}}^\gamma \left[(Q_{\alpha\gamma}^{\mathrm{u}})^2 + (Q_{\beta\gamma}^{\mathrm{u}})^2 - 2Q_{\alpha\gamma}^{\mathrm{u}}Q_{\beta\gamma}^{\mathrm{u}}\,\mathrm{e}^{-a_\gamma^{\mathrm{u}}t}\right]. \tag{F.4}$$

We now consider the process with a single jump at a fixed time $\tau < t$, i.e. we start in the equilibrium of the unfolded u-state and propagate in the u-state from time 0 to τ and in the folded f-state from time τ to t. Averages with respect to this process will be denoted by $\langle\cdot\rangle_{\mathrm{u}\to\mathrm{f}}$. Within the Gaussian network model the center-of-mass motion is independent of the network structure and we obtain similar to above (but now the modes are mixed due to $Q^{\mathrm{u}} \neq Q^{\mathrm{f}}$ and thus no longer decouple),

$$\begin{aligned} \left\langle \left(\vec{R}_t^\alpha - \vec{R}_0^\beta\right)^2 \right\rangle_{\mathrm{u}\overset{\tau}{\to}\mathrm{f}} &= 6D_{\mathrm{COM}}t + \sum_{\gamma,\nu=2}^N \Big[Q_{\alpha\gamma}^{\mathrm{u}}Q_{\alpha\nu}^{\mathrm{u}}\left\langle(\mathbf{X}_t^{\mathrm{f}})_\gamma \cdot (\mathbf{X}_t^{\mathrm{f}})_\nu\right\rangle_{\mathrm{u}\overset{\tau}{\to}\mathrm{f}} \\ &\quad + Q_{\beta\gamma}^{\mathrm{u}}Q_{\beta\nu}^{\mathrm{u}}\left\langle(\mathbf{X}_0^{\mathrm{f}})_\gamma \cdot (\mathbf{X}_0^{\mathrm{f}})_\nu\right\rangle_{\mathrm{u}\overset{\tau}{\to}\mathrm{f}} - 2Q_{\alpha\gamma}^{\mathrm{u}}Q_{\beta\nu}^{\mathrm{u}}\left\langle(\mathbf{X}_t^{\mathrm{f}})_\gamma \cdot (\mathbf{X}_0^{\mathrm{f}})_\nu\right\rangle_{\mathrm{u}\overset{\tau}{\to}\mathrm{f}}\Big]. \end{aligned} \tag{F.5}$$

Now we determine the three terms $\left\langle(\mathbf{X}_t^{\mathrm{f}})_\gamma \cdot (\mathbf{X}_t^{\mathrm{f}})_\nu\right\rangle_{\mathrm{u}\overset{\tau}{\to}\mathrm{f}}$, $\left\langle(\mathbf{X}_0^{\mathrm{f}})_\gamma \cdot (\mathbf{X}_0^{\mathrm{f}})_\nu\right\rangle_{\mathrm{u}\overset{\tau}{\to}\mathrm{f}}$ and $\left\langle(\mathbf{X}_t^{\mathrm{f}})_\gamma \cdot (\mathbf{X}_0^{\mathrm{f}})_\nu\right\rangle_{\mathrm{u}\overset{\tau}{\to}\mathrm{f}}$. The first term resembles $\left\langle(\mathbf{X}_t^{\mathrm{f}})_\gamma(\mathbf{X}_t^{\mathrm{f}})_\nu\right\rangle_{\mathrm{f}} = \delta_{\gamma\nu}V_{\mathrm{f}}^\gamma$ with the difference that we do not start in the f-equilibrium but

propagate the f-process from the u-equilibrium from time τ to t. In particular, modes are mixed since correlations at time τ are only diagonal in u-normal modes $\mathbf{X}^{\mathrm{u}}$ but not in $\mathbf{X}^{\mathrm{f}}$. Using equation (F.2) we have

$$\left\langle (\mathbf{X}_t^{\mathrm{f}})_\gamma \cdot (\mathbf{X}_t^{\mathrm{f}})_\nu \right\rangle_{\mathrm{u}\xrightarrow{\tau}\mathrm{f}} = \left\langle (\mathbf{X}_\tau^{\mathrm{f}})_\gamma \cdot (\mathbf{X}_\tau^{\mathrm{f}})_\nu \right\rangle_{\mathrm{u}\xrightarrow{\tau}\mathrm{f}} \mathrm{e}^{-(a_\gamma+a_\nu)(t-\tau)} + \delta_{\gamma\nu} V^\gamma (t-\tau). \tag{F.6}$$

Since we start in u-equilibrium and propagate in the u-process until time τ, we complete the calculation of the first term by calculating the second term, by expressing f-modes in terms of u-modes. Using the notation $Q^{\mathrm{u}\to\mathrm{f}} \equiv (Q^{\mathrm{f}})^{\mathrm{T}} Q^{\mathrm{u}}$ (s.t. as in $\mathbf{R} = Q^{\mathrm{u}}\mathbf{X}^{\mathrm{u}} = Q^{\mathrm{f}}\mathbf{X}^{\mathrm{f}}$ we have $\mathbf{X}^{\mathrm{f}} = Q^{\mathrm{u}\to\mathrm{f}}\mathbf{X}^{\mathrm{u}}$),

$$\begin{aligned}\left\langle (\mathbf{X}_\tau^{\mathrm{f}})_\gamma \cdot (\mathbf{X}_\tau^{\mathrm{f}})_\nu \right\rangle_{\mathrm{u}\xrightarrow{\tau}\mathrm{f}} &= \left\langle (\mathbf{X}_0^{\mathrm{f}})_\gamma \cdot (\mathbf{X}_0^{\mathrm{f}})_\nu \right\rangle_{\mathrm{u}\xrightarrow{\tau}\mathrm{f}} = \left\langle (\mathbf{X}_0^{\mathrm{f}})_\gamma \cdot (\mathbf{X}_0^{\mathrm{f}})_\nu \right\rangle_{\mathrm{u}} \\ &= \sum_{\omega=2}^{N} Q^{\mathrm{u}\to\mathrm{f}}_{\gamma\omega} Q^{\mathrm{u}\to\mathrm{f}}_{\nu\omega} V^\omega_{\mathrm{u}}.\end{aligned} \tag{F.7}$$

For the third term we employ equation (F.1) for the f-process from time τ to t and for the u-process from 0 to τ,

$$\begin{aligned}\left\langle (\mathbf{X}_t^{\mathrm{f}})_\gamma \cdot (\mathbf{X}_0^{\mathrm{f}})_\nu \right\rangle_{\mathrm{u}\xrightarrow{\tau}\mathrm{f}} &= \mathrm{e}^{-a^{\mathrm{f}}_\gamma (t-\tau)} \left\langle (\mathbf{X}_\tau^{\mathrm{f}})_\gamma \cdot (\mathbf{X}_0^{\mathrm{f}})_\nu \right\rangle_{\mathrm{u}\xrightarrow{\tau}\mathrm{f}} \\ &= \mathrm{e}^{-a^{\mathrm{f}}_\gamma (t-\tau)} \sum_{\omega,\omega'=2}^{N} Q^{\mathrm{u}\to\mathrm{f}}_{\gamma\omega} Q^{\mathrm{u}\to\mathrm{f}}_{\nu\omega'} \left\langle (\mathbf{X}_\tau^{\mathrm{u}})_\omega \cdot (\mathbf{X}_0^{\mathrm{u}})_{\omega'} \right\rangle_{\mathrm{u}} \\ &= \mathrm{e}^{-a^{\mathrm{f}}_\gamma (t-\tau)} \sum_{\omega=2}^{N} Q^{\mathrm{u}\to\mathrm{f}}_{\gamma\omega} Q^{\mathrm{u}\to\mathrm{f}}_{\nu\omega} V^\omega_{\mathrm{u}}\, \mathrm{e}^{-a^{\mathrm{u}}_\omega \tau}.\end{aligned} \tag{F.8}$$

Combining equations (F.5) and (F.8) and using $\sum_{\gamma\nu} C_\gamma C_\nu = (\sum_\gamma C_\gamma)^2$ and for the last term $Q^{\mathrm{f}} Q^{\mathrm{u}\to\mathrm{f}} = Q^{\mathrm{u}}$ we arrive at the result equation (22),

$$\begin{aligned}\left\langle \left(\vec{R}_t^{\,\alpha} - \vec{R}_0^{\,\beta}\right)^2 \right\rangle_{\mathrm{u}\xrightarrow{\tau}\mathrm{f}} &= 6 D_{\mathrm{COM}} t + \sum_{\gamma=2}^{N} (Q^{\mathrm{u}}_{\beta\gamma})^2 V^\gamma_{\mathrm{u}} + \sum_{\gamma=2}^{N} (Q^{\mathrm{f}}_{\alpha\gamma})^2 V^\gamma_{\mathrm{f}} (t-\tau) \\ &+ \sum_{\omega=2}^{N} V^\omega_{\mathrm{u}} \left[\sum_{\gamma=2}^{N} Q^{\mathrm{f}}_{\alpha\gamma} Q^{\mathrm{u}\to\mathrm{f}}_{\gamma\omega}\, \mathrm{e}^{-a^{\mathrm{f}}_\gamma (t-\tau)} \right]^2 - 2 \sum_{\omega,\gamma=2}^{N} Q^{\mathrm{f}}_{\alpha\omega} Q^{\mathrm{u}\to\mathrm{f}}_{\omega\gamma} Q^{\mathrm{u}}_{\beta\gamma} V^\gamma_{\mathrm{u}}\, \mathrm{e}^{-a^{\mathrm{f}}_\omega (t-\tau) - a^{\mathrm{u}}_\gamma \tau}.\end{aligned} \tag{F.9}$$

Finally, for completeness we here show the Kirchoff matrix A^{f} corresponding to the Trp-cage miniprotein construct TC5b (PDB: 1L2Y)

$$A^{\mathrm{f}} = \frac{k}{\xi} \begin{bmatrix}
6 & -1 & -1 & -1 & -1 & -1 & -1 & 0 & 0 & 0 & 0 & 0 & 0 & 0 & 0 & 0 & 0 & 0 & 0 & 0 \\
-1 & 9 & -1 & -1 & -1 & -1 & -1 & 0 & 0 & 0 & 0 & 0 & 0 & 0 & 0 & 0 & 0 & -1 & -1 & -1 \\
-1 & -1 & 11 & -1 & -1 & -1 & -1 & -1 & 0 & 0 & -1 & 0 & 0 & 0 & 0 & 0 & 0 & -1 & -1 & -1 \\
-1 & -1 & -1 & 10 & -1 & -1 & -1 & -1 & -1 & 0 & -1 & 0 & 0 & 0 & 0 & 0 & 0 & 0 & -1 & 0 \\
-1 & -1 & -1 & -1 & 11 & -1 & -1 & -1 & -1 & -1 & -1 & 0 & 0 & 0 & 0 & 0 & 0 & 0 & -1 & 0 \\
-1 & -1 & -1 & -1 & -1 & 16 & -1 & -1 & -1 & -1 & -1 & -1 & 0 & -1 & 0 & -1 & -1 & -1 & -1 & 0 \\
-1 & -1 & -1 & -1 & -1 & -1 & 14 & -1 & -1 & -1 & -1 & -1 & -1 & -1 & 0 & 0 & 0 & -1 & 0 & 0 \\
0 & 0 & -1 & -1 & -1 & -1 & -1 & 9 & -1 & -1 & -1 & 0 & 0 & -1 & 0 & 0 & 0 & 0 & 0 & 0 \\
0 & 0 & 0 & -1 & -1 & -1 & -1 & -1 & 12 & -1 & -1 & -1 & -1 & -1 & -1 & -1 & 0 & 0 & 0 & 0 \\
0 & 0 & 0 & 0 & -1 & -1 & -1 & -1 & -1 & 11 & -1 & -1 & -1 & -1 & -1 & -1 & 0 & 0 & 0 & 0 \\
0 & 0 & -1 & -1 & -1 & -1 & -1 & -1 & -1 & -1 & 15 & -1 & -1 & -1 & -1 & -1 & -1 & -1 & 0 & 0 \\
0 & 0 & 0 & 0 & 0 & -1 & -1 & 0 & -1 & -1 & -1 & 11 & -1 & -1 & -1 & -1 & -1 & -1 & 0 & 0 \\
0 & 0 & 0 & 0 & 0 & 0 & -1 & 0 & -1 & -1 & -1 & -1 & 9 & -1 & -1 & -1 & -1 & 0 & 0 & 0 \\
0 & 0 & 0 & 0 & 0 & -1 & -1 & -1 & -1 & -1 & -1 & -1 & -1 & 11 & -1 & -1 & -1 & 0 & 0 & 0 \\
0 & 0 & 0 & 0 & 0 & 0 & 0 & 0 & -1 & -1 & -1 & -1 & -1 & -1 & 8 & -1 & -1 & 0 & 0 & 0 \\
0 & 0 & 0 & 0 & 0 & -1 & 0 & 0 & -1 & -1 & -1 & -1 & -1 & -1 & -1 & 11 & -1 & -1 & -1 & 0 \\
0 & 0 & 0 & 0 & 0 & -1 & 0 & 0 & 0 & 0 & -1 & -1 & -1 & -1 & -1 & -1 & 10 & -1 & -1 & -1 \\
0 & -1 & -1 & 0 & 0 & -1 & -1 & 0 & 0 & 0 & -1 & -1 & 0 & 0 & 0 & -1 & -1 & 10 & -1 & -1 \\
0 & -1 & -1 & -1 & -1 & -1 & 0 & 0 & 0 & 0 & 0 & 0 & 0 & 0 & 0 & -1 & -1 & -1 & 9 & -1 \\
0 & -1 & -1 & 0 & 0 & 0 & 0 & 0 & 0 & 0 & 0 & 0 & 0 & 0 & 0 & 0 & -1 & -1 & -1 & 5
\end{bmatrix}, \tag{F.10}$$

and the 20×20 tridiagonal Kirchoff matrix A^{u} for the unfolded Rouse chain

$$A^{\mathrm{u}} = \frac{k}{\xi}\begin{bmatrix} 1 & -1 & & & & & \\ -1 & 2 & -1 & & & 0 & \\ & -1 & 2 & -1 & & & \\ & & & \cdots & \cdots & & \\ & & & & \cdots & \cdots & \\ & 0 & & & -1 & 2 & -1 \\ & & & & & -1 & 1 \end{bmatrix}. \tag{F.11}$$

ORCID iDs

Cai Dieball https://orcid.org/0000-0002-0011-2358
Diego Krapf https://orcid.org/0000-0002-2833-5553
Matthias Weiss https://orcid.org/0000-0001-8814-9915
Aljaž Godec https://orcid.org/0000-0003-1888-6666

References

[1] Bouchaud J-P and Georges A 1990 Anomalous diffusion in disordered media: statistical mechanisms, models and physical applications *Phys. Rep.* **195** 127
[2] Barkai E, Garini Y and Metzler R 2012 Strange kinetics of single molecules in living cells *Phys. Today* **65** 29
[3] Höfling F and Franosch T 2013 Anomalous transport in the crowded world of biological cells *Rep. Prog. Phys.* **76** 046602
[4] Krapf D 2015 Mechanisms underlying anomalous diffusion in the plasma membrane *Curr. Top. Membr.* **75** 167
[5] Jeon J-H, Javanainen M, Martinez-Seara H, Metzler R and Vattulainen I 2016 Protein crowding in lipid bilayers gives rise to non-Gaussian anomalous lateral diffusion of phospholipids and proteins *Phys. Rev.* X **6** 021006
[6] Guigas G and Weiss M 2008 Sampling the cell with anomalous diffusion—the discovery of slowness *Biophys. J.* **94** 90
[7] McKinley S A, Yao L and Forest M G 2009 Transient anomalous diffusion of tracer particles in soft matter *J. Rheol.* **53** 1487
[8] Tolić-Nørrelykke I M, Munteanu E-L, Thon G, Oddershede L and Berg-Sørensen K 2004 Anomalous diffusion in living yeast cells *Phys. Rev. Lett.* **93** 078102
[9] Wong I Y, Gardel M L, Reichman D R, Weeks E R, Valentine M T, Bausch A R and Weitz D A 2004 Anomalous diffusion probes microstructure dynamics of entangled F-actin networks *Phys. Rev. Lett.* **92** 178101
[10] Godec A, Bauer M and Metzler R 2014 Collective dynamics effect transient subdiffusion of inert tracers in flexible gel networks *New J. Phys.* **16** 092002
[11] Chubynsky M V and Slater G W 2014 Diffusing diffusivity: a model for anomalous, yet Brownian, diffusion *Phys. Rev. Lett.* **113** 098302
[12] Chechkin A V, Seno F, Metzler R and Sokolov I M 2017 Brownian yet non-Gaussian diffusion: from superstatistics to subordination of diffusing diffusivities *Phys. Rev.* X **7** 021002
[13] Metzler R, Jeon J-H, Cherstvy A G and Barkai E 2014 Anomalous diffusion models and their properties: non-stationarity, non-ergodicity, and ageing at the centenary of single particle tracking *Phys. Chem. Chem. Phys.* **16** 24128
[14] Manzo C and Garcia-Parajo M F 2015 A review of progress in single particle tracking: from methods to biophysical insights *Rep. Prog. Phys.* **78** 124601
[15] Meroz Y and Sokolov I M 2015 A toolbox for determining subdiffusive mechanisms *Phys. Rep.* **573** 1–29
[16] Szabo A, Shoup D, Northrup S H and McCammon J A 1982 Stochastically gated diffusion-influenced reactions *J. Chem. Phys.* **77** 4484
[17] Zwanzig R 1992 Dynamical disorder: passage through a fluctuating bottleneck *J. Chem. Phys.* **97** 3587
[18] Bier M and Astumian R D 1993 Matching a diffusive and a kinetic approach for escape over a fluctuating barrier *Phys. Rev. Lett.* **71** 1649
[19] Doering C R and Gadoua J C 1992 Resonant activation over a fluctuating barrier *Phys. Rev. Lett.* **69** 2318
[20] Godec A and Metzler R 2017 First passage time statistics for two-channel diffusion *J. Phys. A: Math. Theor.* **50** 084001
[21] Wunderlich Z and Mirny L A 2008 Spatial effects on the speed and reliability of protein-DNA search *Nucl. Acids Res.* **36** 3570
[22] Koslover E F, Díaz de la Rosa M A and Spakowitz A J 2011 Theoretical and computational modeling of target-site search kinetics *in vitro* and *in vivo Biophys. J.* **101** 856
[23] Sheinman M, Bénichou O, Kafri Y and Voituriez R 2012 Classes of fast and specific search mechanisms for proteins on DNA *Rep. Prog. Phys.* **75** 026601
[24] Yamamoto E, Akimoto T, Mitsutake A and Metzler R 2021 Universal relation between instantaneous diffusivity and radius of gyration of proteins in aqueous solution *Phys. Rev. Lett.* **126** 128101
[25] Baldovin F, Orlandini E and Seno F 2019 Polymerization induces non-Gaussian diffusion *Front. Phys.* **7** 124
[26] Maizón H B and Barrantes F J 2021 A deep learning-based approach to model anomalous diffusion of membrane proteins: the case of the nicotinic acetylcholine receptor *Briefings Bioinf.* bbab435
[27] Kärger J 1985 NMR self-diffusion studies in heterogeneous systems *Adv. Colloid Interface Sci.* **23** 129
[28] Grebenkov D S 2019 Time-averaged mean square displacement for switching diffusion *Phys. Rev.* E **99** 032133
[29] Sabri A, Xu X, Krapf D and Weiss M 2020 Elucidating the origin of heterogeneous anomalous diffusion in the cytoplasm of mammalian cells *Phys. Rev. Lett.* **125** 058101
[30] Janczura J, Balcerek M, Burnecki K, Sabri A, Weiss M and Krapf D 2021 Identifying heterogeneous diffusion states in the cytoplasm by a hidden Markov model *New J. Phys.* **23** 053018
[31] Ernst D, Köhler J and Weiss M 2014 Probing the type of anomalous diffusion with single-particle tracking *Phys. Chem. Chem. Phys.* **16** 7686

[32] Woringer M, Izeddin I, Favard C and Berry H 2020 Anomalous subdiffusion in living cells: bridging the gap between experiments and realistic models through collaborative challenges *Front. Phys.* **8** 134
[33] Sikora G, Wyłomańska A, Gajda J, Solé L, Akin E J, Tamkun M M and Krapf D 2017 Elucidating distinct ion channel populations on the surface of hippocampal neurons via single-particle tracking recurrence analysis *Phys. Rev.* E **96** 062404
[34] Akimoto T and Yamamoto E 2017 Detection of transition times from single-particle-tracking trajectories *Phys. Rev.* E **96** 052138
[35] Lanoiselée Y and Grebenkov D S 2017 Unraveling intermittent features in single-particle trajectories by a local convex hull method *Phys. Rev.* E **96** 022144
[36] Zaccai G 2000 How soft is a protein? A protein dynamics force constant measured by neutron scattering *Science* **288** 1604
[37] Kneller G R 2005 Quasielastic neutron scattering and relaxation processes in proteins: analytical and simulation-based models *Phys. Chem. Chem. Phys.* **7** 2641
[38] Biehl R, Monkenbusch M and Richter D 2011 Exploring internal protein dynamics by neutron spin echo spectroscopy *Soft Matter* **7** 1299
[39] Martel P 1992 Biophysical aspects of neutron scattering from vibrational modes of proteins *Prog. Biophys. Mol. Biol.* **57** 129
[40] van Hove L 1954 Correlations in space and time and Born approximation scattering in systems of interacting particles *Phys. Rev.* **95** 249
[41] Mezei F, Pappas C and Gutberlet T (ed) 2002 *Neutron Spin Echo Spectroscopy: Basics, Trends, and Applications* (*Lecture Notes in Physics* vol 601) (Berlin: Springer)
[42] Richter D, Monkenbusch M, Arbe A and Colmenero J 2005 *Neutron Spin Echo in Polymer Systems* (Berlin: Springer)
[43] Callaway D J and Bu Z 2017 Visualizing the nanoscale: protein internal dynamics and neutron spin echo spectroscopy *Curr. Opin. Struct. Biol.* **42** 1–5
[44] Liu Y 2017 Intermediate scattering function for macromolecules in solutions probed by neutron spin echo *Phys. Rev.* E **95** 020501
[45] Kurzthaler C, Devailly C, Arlt J, Franosch T, Poon W C K, Martinez V A and Brown A T 2018 Probing the spatiotemporal dynamics of catalytic Janus particles with single-particle tracking and differential dynamic microscopy *Phys. Rev. Lett.* **121** 078001
[46] Cerbino R and Trappe V 2008 Differential dynamic microscopy: probing wave vector dependent dynamics with a microscope *Phys. Rev. Lett.* **100** 188102
[47] Wilson L G, Martinez V A, Schwarz-Linek J, Tailleur J, Bryant G, Pusey P N and Poon W C K 2011 Differential dynamic microscopy of bacterial motility *Phys. Rev. Lett.* **106** 018101
[48] Senning E N and Marcus A H 2010 Subcellular dynamics and protein conformation fluctuations measured by Fourier imaging correlation spectroscopy *Annu. Rev. Phys. Chem.* **61** 111
[49] Knowles M, Grassman T and Marcus A 2000 Measurement of the dynamic structure function of fluorescently labeled complex fluids by Fourier imaging correlation spectroscopy *Phys. Rev. Lett.* **85** 2837
[50] Kolin D L, Ronis D and Wiseman P W 2006 *k*-space image correlation spectroscopy: a method for accurate transport measurements independent of fluorophore photophysics *Biophys. J.* **91** 3061
[51] Monkenbusch M *et al* 2016 Molecular view on supramolecular chain and association dynamics *Phys. Rev. Lett.* **117** 147802
[52] Hansen J-P and McDonald I R 2013 *Theory of Simple Liquids* 4th edn (New York: Academic)
[53] Réat V, Patzelt H, Ferrand M, Pfister C, Oesterhelt D and Zaccai G 1998 Dynamics of different functional parts of bacteriorhodopsin: H-2H labeling and neutron scattering *Proc. Natl Acad. Sci. USA* **95** 4970
[54] Singwi K S and Sjölander A 1960 Diffusive motions in water and cold neutron scattering *Phys. Rev.* **119** 863
[55] Postnikov E B, Chechkin A and Sokolov I M 2020 Brownian yet non-Gaussian diffusion in heterogeneous media: from superstatistics to homogenization *New J. Phys.* **22** 063046
[56] Weiss M 2014 Crowding, diffusion, and biochemical reactions *Int. Rev. Cell Mol. Biol.* **307** 383
[57] Smoluchowski M V 1916 Drei Vortraege uber Diffusion, Brownsche Bewegung und Koagulation von Kolloidteilchen *Phys. Z.* **17** 557–85
[58] Collins F C and Kimball G E 1949 Diffusion-controlled reaction rates *J. Colloid Sci.* **4** 425
[59] Uhlenbeck G E and Ornstein L S 1930 On the theory of the Brownian motion *Phys. Rev.* **36** 823
[60] Bateman H and Erdélyi A 1955 *Higher Transcendental Functions Volume 1: Bateman Manuscript Project* (New York, NY: McGraw-Hill)
[61] Matsarskaia O, Bühl L, Beck C, Grimaldo M, Schweins R, Zhang F, Seydel T, Schreiber F and Roosen-Runge F 2020 Evolution of the structure and dynamics of bovine serum albumin induced by thermal denaturation *Phys. Chem. Chem. Phys.* **22** 18507
[62] Henry L, Panman M R, Isaksson L, Claesson E, Kosheleva I, Henning R, Westenhoff S and Berntsson O 2020 Real-time tracking of protein unfolding with time-resolved x-ray solution scattering *Struct. Dyn.* **7** 054702
[63] Kim T W *et al* 2020 Protein folding from heterogeneous unfolded state revealed by time-resolved x-ray solution scattering *Proc. Natl Acad. Sci. USA* **117** 14996
[64] Lapolla A, Vossel M and Godec A 2021 Time- and ensemble-average statistical mechanics of the Gaussian network model *J. Phys. A: Math. Theor.* **54** 355601
[65] Haliloglu T, Bahar I and Erman B 1997 Gaussian dynamics of folded proteins *Phys. Rev. Lett.* **79** 3090
[66] Bakan A, Meireles L M and Bahar I 2011 ProDy: protein dynamics inferred from theory and experiments *Bioinformatics* **27** 1575
[67] Rouse P E 1953 A theory of the linear viscoelastic properties of dilute solutions of coiling polymers *J. Chem. Phys.* **21** 1272
[68] Doi M and Edwards S F 1988 *The Theory of Polymer Dynamics* (*International Series of Monographs on Physics*) (Oxford: Clarendon)
[69] Lapolla A and Godec A 2020 Faster uphill relaxation in thermodynamically equidistant temperature quenches *Phys. Rev. Lett.* **125** 110602
[70] Cheng R R, Hawk A T and Makarov D E 2013 Exploring the role of internal friction in the dynamics of unfolded proteins using simple polymer models *J. Chem. Phys.* **138** 074112
[71] Zimm B H 1956 Dynamics of polymer molecules in dilute solution: viscoelasticity, flow birefringence and dielectric loss *J. Chem. Phys.* **24** 269
[72] Granek R and Cates M E 1992 Stress relaxation in living polymers: results from a Poisson renewal model *J. Chem. Phys.* **96** 4758
[73] Stukalin E B and Freed K F 2006 Minimal model of relaxation in an associating fluid: viscoelastic and dielectric relaxations in equilibrium polymer solutions *J. Chem. Phys.* **125** 184905
[74] Hartich D and Godec A 2021 Emergent memory and kinetic hysteresis in strongly driven networks *Phys. Rev.* X **11** 041047
[75] Krapf D and Metzler R 2019 Strange interfacial molecular dynamics *Phys. Today* **72** 48–54

[76] Weron A, Burnecki K, Akin E J, Solé L, Balcerek M, Tamkun M M and Krapf D 2017 Ergodicity breaking on the neuronal surface emerges from random switching between diffusive states *Sci. Rep.* **7** 5404
[77] Wuttke J 2012 Laplace–Fourier transform of the stretched exponential function: analytic error bounds, double exponential transform, and open-source implementation 'libkww' *Algorithms* **5** 604
[78] Prudnikov A P, Brychkov Y A and Marichev O I 1992 *Integrals and Series: Direct Laplace Transforms* vol 4 (London: Gordon and Breach)
[79] Davies R B and Harte D S 1987 Tests for Hurst effect *Biometrika* **74** 95
[80] Doob J L 1953 *Stochastic Processes* (New York: Wiley)